Opto-Electronic Advances

Review

2021, Vol. 4, No. 3

DOI: 10.29026/oea.2021.200045

Review of micromachined optical accelerometers: from m*g* to sub-µ*g*

Qianbo Lu[1,2†*], Yinan Wang[3†], Xiaoxu Wang[3], Yuan Yao[4], Xuewen Wang[1,2] and Wei Huang[1,2*]

Micro-Opto-Electro-Mechanical Systems (MOEMS) accelerometer is a new type of accelerometer which combines the merits of optical measurement and Micro-Electro-Mechanical Systems (MEMS) to enable high precision, small volume and anti-electromagnetic disturbance measurement of acceleration. In recent years, with the in-depth research and development of MOEMS accelerometers, the community is flourishing with the possible applications in seismic monitoring, inertial navigation, aerospace and other industrial and military fields. There have been a variety of schemes of MOEMS accelerometers, whereas the performances differ greatly due to different measurement principles and corresponding application requirements. This paper aims to address the pressing issue of the current lack of systematic review of MOEMS accelerometers. According to the optical measurement principle, we divide the MOEMS accelerometers into three categories: the geometric optics based, the wave optics based, and the new optomechanical accelerometers. Regarding the most widely studied category, the wave optics based accelerometers are further divided into four sub-categories, which is based on grating interferometric cavity, Fiber Bragg Grating (FBG), Fabry-Perot cavity, and photonic crystal, respectively. Following a brief introduction to the measurement principles, the typical performances, advantages and disadvantages as well as the potential application scenarios of all kinds of MOEMS accelerometers are discussed on the basis of typical demonstrations. This paper also presents the status and development tendency of MOEMS accelerometers to meet the ever-increasing demand for high-precision acceleration measurement.

Keywords: accelerometer; Micro-Opto-Electro-Mechanical Systems (MOEMS); integrated optics; accelerometer review

Lu QB, Wang YN, Wang XX, Yao Y, Wang XW et al. Review of micromachined optical accelerometers: from m*g* to sub-µ*g*. *Opto-Electron Adv* **4**, 200045 (2021).

Introduction

As graduations of a scale for acceleration, velocity and position measurement, accelerometer is not only a key component of the inertial navigation system, but also plays a vital role in a broad spectrum of applications such as automobile safety, earthquake monitoring, gravity detection, heading indication, attitude reference. With the rapid development of microelectronics and micro-manufacturing technology, high performance and highly integrated MEMS accelerometers have become a big class of accelerometers, which covers the applications in consumer electronics, industry, medical treatment, etc. Due to the growing demand for higher performance and greater functionality, MOEMS accelerometers emerged at the right moment, combining the advantages of optical detection and traditional MEMS accelerometers. Compared to conventional MEMS accelerometers, MOEMS accelerometers are usually with advanctages of high

[1]Frontiers Science Center for Flexible Electronics (FSCFE), Shaanxi Institute of Flexible Electronics (SIFE) & Shaanxi Institute of Biomedical Materials and Engineering (SIBME), Northwestern Polytechnical University, Xi'an 710072, China; [2]MIIT Key Laboratory of Flexible Electronics (KLoFE), Northwestern Polytechnical University, Xi'an 710072, China; [3]The Key Laboratory of Information Fusion Technology, Ministry of Education, School of Automation, Northwestern Polytechnical University, Xi'an 710072, China; [4]Wuhan National Laboratory for Optoelectronics-Huazhong University of Science and Technology, Wuhan 430074, China.

[†]These authors contributed equally to this work.

[*]Correspondence: QB Lu, E-mail: iamqlu@nwpu.edu.cn; W Huang, E-mail: iamwhuang@nwpu.edu.cn

Received: 17 August 2020; Accepted: 23 September 2020; Published: 25 March 2021

precision, fast response, resistance to electromagnetic interference, and the ability to work in harsh environments. Therefore, they show promise for broad application prospect in inertial navigation, geophysics and other fields that require high sensitivity and precision, and are also the trend of future accelerometers development.

Various MOEMS accelerometers have been reported in past decades, yet a systematical review of the MOEMS accelerometers has remained elusive. In this review, we mainly focus on the measurement principle and performance of state-of-the-art MOEMS accelerometers, and divide them into several categories according to the optical measurement principle. By taking typical demonstrations as examples, the merits and disadvantages are presented here, thereby drawing a big picture for MOEMS accelerometers, along with their application prospect and development tendency.

Requirement analysis of MOEMS accelerometers

The application of MOEMS accelerometers spans a wide variety of areas, while different application scenarios have different requirements on performances. As illustrated in Fig. 1, for example, microgravity detection[1] requires extremely high acceleration sensitivity (sub-μGal), excellent long-term stability and superior low frequency response, inertial navigation system[2] requires low noise level and good zero-bias stability (sub-μ*g*), whereas large bandwidth is crucial in acoustic and vibration measurement applications[3]. The requirements of some typical applications will be reviewed here.

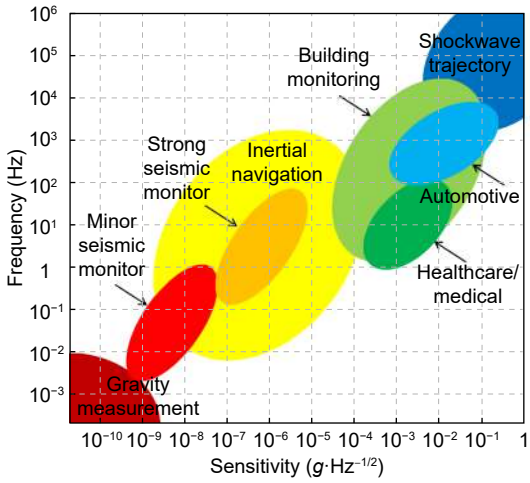

Fig. 1 | Typical specifications of potential application scenarios of MOEMS accelerometers.

Application of inertial navigation

Based on Newtonian mechanics law, the inertial navigation system measures the acceleration and angular acceleration of the carrier, taking the time integral and then transforms the obtained data into the navigation coordinate system to obtain the velocity, yaw angle and position information. Accelerometer is one of the key components of the inertial navigation system. The working environment of inertial navigation system includes air, ground and underwater, which requires the accelerometer to have a strong anti-environment disturbance ability. For inertial guidance long-range missiles, 70% of the precision depends on the guidance system. This poses a significant challenge for the accelerometer to feature an excellent acceleration measurement precision and zero bias stability. Also, the size of the inertial navigation system as well as the accelerometer should be considered due to the limited carrying capacity of various aircrafts and underwater vehicles. Because of the advantages of high precision, small size and anti-electromagnetic interference, MOEMS accelerometers have good prospects for the application of inertial navigation.

Application of building monitoring

Small deformation would cause cracks or other catastrophic losses in structures such as buildings and bridges. Accelerometer can help detect flaws and give early warning by measuring the vibration of buildings, thus, playing a key role in the building monitoring system. There are some limitations of traditional accelerometers in such applications due to their complicated wiring, difficulty in multi-point measurement and electromagnetic susceptibility. As a comparison, MOEMS accelerometers have strong anti-electromagnetic disturbance ability and higher precision, and some types of MOEMS accelerometers such as fiber grating based accelerometers can realize long-distance and distributed measurement, which helps to break through these limitations[4]. Therefore, MOEMS accelerometers have potential for large-scale applications in structural health detection of buildings and bridges, as well as vibration detection of aircraft wings[5].

Geophysical applications

Geophysical applications mainly contain seismic, drilling process monitoring, resource exploration, monitoring of earth tides and volcanic activity, etc. The seismic

monitoring, which can be further divided into minor and strong seismic monitoring, requires a noise level of better than 1 $ng \cdot Hz^{-1/2}$ and 1 $\mu g \cdot Hz^{-1/2}$, respectively, and the frequency band shall cover 0.0083–50 Hz. Drilling monitoring includes transverse, axial and torsional vibration measurement. Gravity based applications such as resource exploration, gravity-aided navigation, earth tides and volcanic activity monitoring, pose a challenge to ultra-high sensitivity and superior low frequency response. Accelerometer is the core component of a gravimeter, so that high performance MOEMS accelerometers would have a broad prospect in such applications[6].

Daily applications

Automotive electronics

In the field of automotive electronics, typical applications including airbag, anti-skid brake system, electric suspension, navigation control all require acceleration measurement. Automotive electronics applications usually do not need a high precision but have a high demand for size and cost. Thus, several MOEMS accelerometers with simple structure and low cost, such as light intensity based accelerometers, can be well applied in such scenes.

Movement monitoring

Motion monitoring makes use of the output value of the accelerometer to build the connection between the output and the daily exercise of human body, such as sitting, standing, running, jumping, and cycling with the help of skin temperature, heart rate and other information obtained from different sensors. This helps to provide professional training assistance and guidance for the subjects, so as to achieve accurate adjustment of training volume and intensity. Due to the long running time, the accelerometers are required to feature good long-term stability and low power consumption.

Medical diagnosis

Accelerometers can be used to assist diagnosis and treatment of patients with motor disorders or joint problems. Similar to motion monitoring, this kind of application puts requirements on accelerometer with good ductility and long-term stability, as well as low power consumption. Optical fiber based MOEMS accelerometers which are adapted to different environmental conditions might be feasible in this application.

Different MOEMS accelerometer types

As shown in Fig. 2, a MOEMS accelerometer usually consists of an acceleration sensing structure and an optical displacement measurement unit. The former is to convert the applied acceleration to a displacement, whereas the latter one is to detect the displacement. The performance of two parts determine the overall performance of the accelerometer together. In this paper, the MOEMS accelerometers are broadly divided in three categories according to the principles of optical displacement measurement unit.

Since the birth of the first optical accelerometer[7,8], MOEMS accelerometers have seen a steady improvement in both the micro-manufacturing technology and optical measurement principle. Regarding the manufacturing technology, the emerging techniques[9,10] such as additive manufacturing[11–13] and SOI-MEMS technology[14] open a path towards high performance and multifunctional MOEMS accelerometers. While the optical measurement principles, go through three stages in general, from the geometric optics schemes based on light intensity, to the wave optics based schemes (based on wavelength, frequency, phase, etc.), and recently to the light-matter interaction based new optomechanical schemes, as shown in Fig. 2. The precision is also improved with the innovation of measurement principle and the advances in technology. The geometric optics based scheme measures the displacement of a proof mass under the application of an external acceleration through variation of the amplitude or intensity of light, thus obtaining the magnitude of the acceleration. This scheme usually has a simple structure along with a large dynamic range, but is with limited precision. Compared with the geometric optics based scheme, the wave optics based schemes yield a profound improvement of precision. Wave optics based schemes can usually be explained by scalar diffraction theory approximation, and they are such a kind of optical accelerometers that have been studied most and widely used at present. The new optomechanical schemes make use of the basic mechanism of the interaction between light and matter at the nanoscale, which can push the sensitivity beyond the state of the art, or even exceed the standard quantum limit (SQL). This kind of MOEMS accelerometer came into being later but holds the promise of ultra-high performances, and most of the schemes are in the stage of principle verification and rapid development.

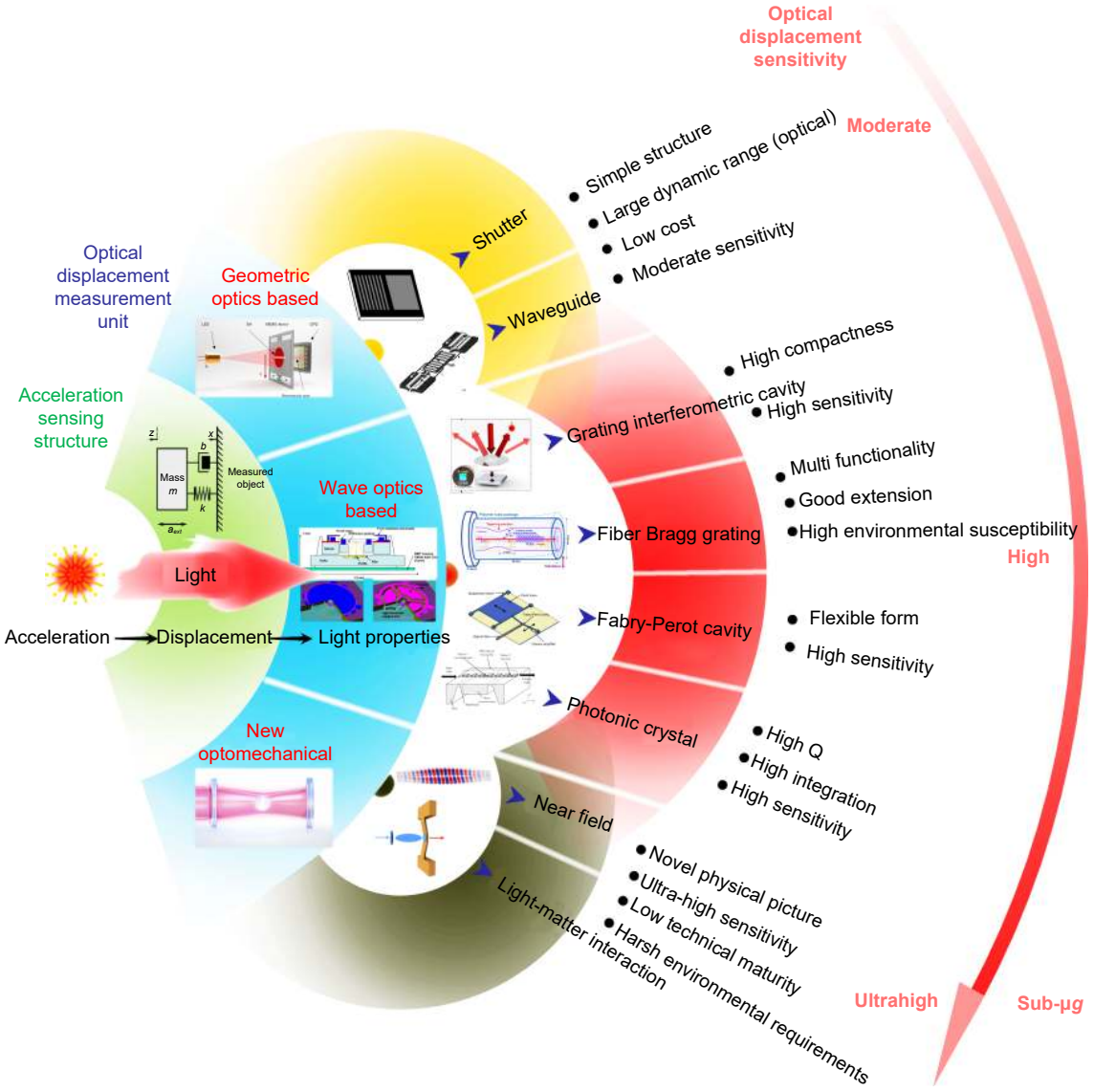

Fig. 2 | Summary of classification of MOEMS accelerometers showing their optical sensing units and figures of merit.

Geometric optics based MOEMS accelerometers

Principle

Geometric optics based MOEMS accelerometer is a kind of accelerometer which senses the displacement or acceleration by directly modulating the radiation intensity of light. As it is subject to acceleration, the proof mass in the accelerometer generates an inertia displacement, which directly changes the output light intensity. In conjunction with the acceleration-displacement sensitivity of the acceleration sensing structure, it is able to calculate the magnitude of the input acceleration. This kind of MOEMS accelerometer has advantages of simple structure and low cost, but it is usually difficult to guarantee its precision due to the relatively high susceptibility to the fluctuation of incident light source and external environment.

Light-intensity based accelerometers

One of the first reported geometric optics based accelerometer was proposed by Abbaspour-Sani et al.[8], and the schematic is shown in Fig. 3. The measurement principle is as follows: an LED source emits light vertically, while the light flux received by the diode changes accordingly with the lateral displacement of the shutter in terms of external acceleration. Two photodetectors containing dark and transparent fringes are placed in light and dark environments, respectively, to achieve a common mode suppression to compensates the temperature drift of the detector. The accelerometer has a linear response range of ±84 *g*, a resonant frequency of 3.2 kHz, while the sensitivity is less accurate than 0.1 V/*g*. Similar grating shutter based demonstrations[15,16] hold advantages of simple

setup and low cost, but the performance cannot meet the high precision requirement.

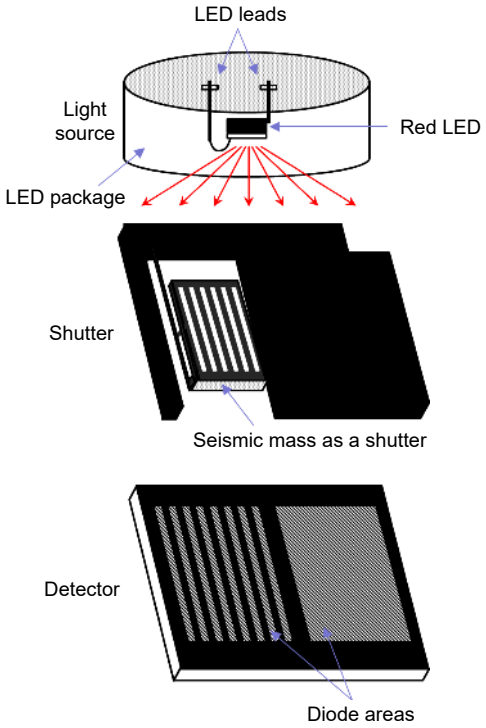

Fig. 3 | Structure of a MOEMS accelerometer based on light intensity. Figure reproduced with permission from ref.[8], IEEE.

Except the grating shutter, waveguides can also be exploited to serve as the light intensity modulation component of an accelerometer. In 2004, Plaza et al.[17] designed a light intensity detection scheme based on waveguides. As shown in Fig. 4, a mass is connected to the frame by four beams, and a waveguide is attached to the mass as a sensing element, self-aligning with the input and output waveguides on the frame. The proof mass shifts along the *z* axis when subjected to a vertical acceleration, which will cause two misalignments, and then modulate the light intensity. The mechanical sensitivity is around 1 μm/*g*, and the optical sensitivity in both positive and negative directions are 169.824%/*g* and 147.911%/*g*, respectively. The accelerometer has the advantage of capability of measuring acceleration in two different directions with a reduced potential stress due to the mechanical design. However, the application of this type of accelerometers remains limited by the high environmental susceptibility and relatively low precision[18–21], as shown in Fig.5.

It can be seen that most of the light intensity based accelerometers hold a simple light path and low sensitivity, but there still are several avenues to improve the sensitivity. For example, as what conventional MEMS accelero-

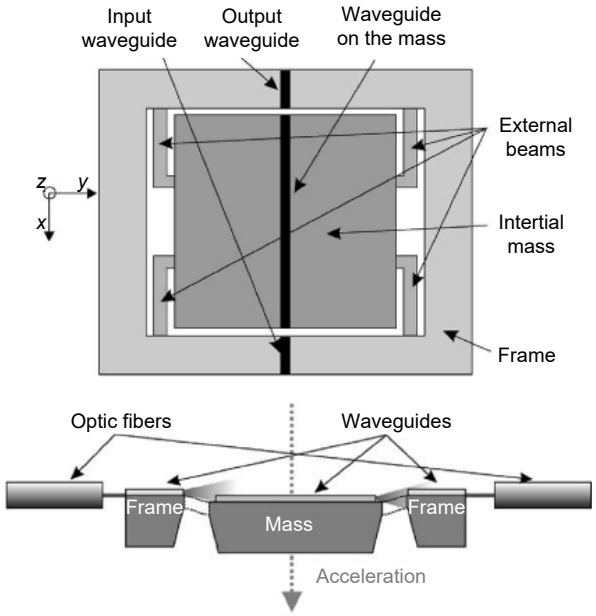

Fig. 4 | Simplified model of a MOEMS accelerometer based on light intensity. Figure reproduced with permission from ref.[17], IEEE.

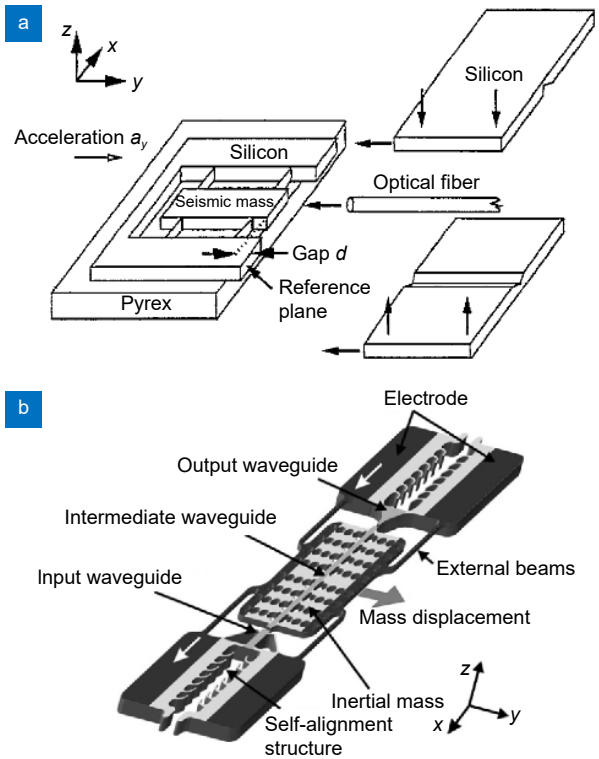

Fig. 5 | (**a**) Schematic of a light intensity based MOEMS accelerometer by using waveguide. (**b**) Schematic view of the MOEMS accelerometer based on waveguide. Figure reproduced with permission from: (a) ref.[18], Elsevier; (b) ref.[19], Elsevier.

meters did[22–24], modifying the mechanical design[25–28] to construct an ultra-sensitive mass-spring system is an effective way, even though it has compromise among the sensitivity and bandwidth, as well as dynamic range. In

2016, Hammond et al.[23] reported an accelerometer based on a geometric anti-spring system. As shown in Fig. 6, the proof mass is suspended to a rigid frame by a spring system, whose elastic constant changes with the displacement of the mass. The accelerometer has an extremely low resonant frequency and high acceleration-displacement sensitivity. When the accelerometer works, the inertia displacement of the proof mass adjusts the light flux, and then changes the current output of the photodiode. The sensitivity of the accelerometer can reach down to 41 $ng \cdot Hz^{-1/2}$ due to its extremely low elastic constant.

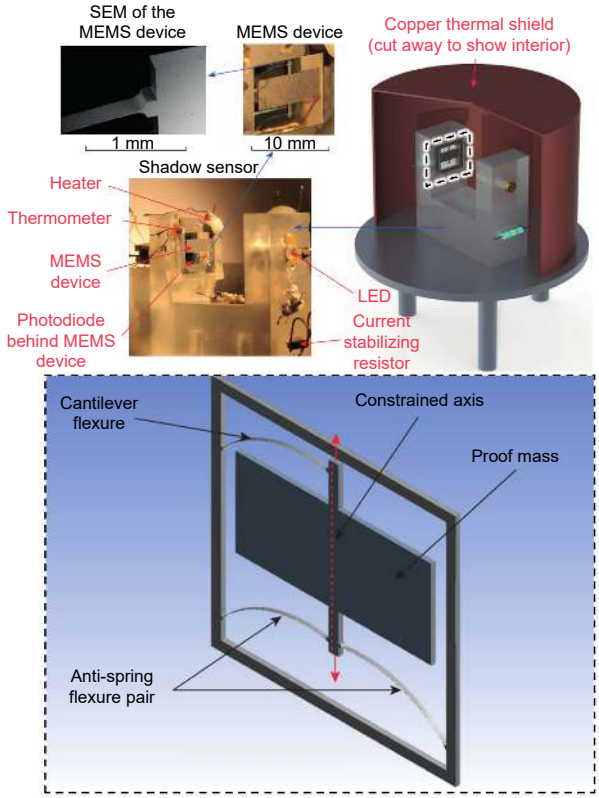

Fig. 6 | The experimental setup along with the mechanics. Figure reproduced with permission from ref.[23], Springer Nature.

Similarly, Tu et al.[24] put forward an ultra-sensitive light intensity based accelerometer later in 2019. An asymmetrical spring system, which is composed of two curved beams and two folded beams, serves as the connection between the proof mass and the frame, providing the ultra-high acceleration-displacement sensitivity. A slit is located in the center of the proof mass, as shown in Fig. 7, so that the light flux through it can change with the displacement of the proof mass, thus changing the output of the quadrant diode. The sensitivity of the accelerometer is down to 8.16 $ng \cdot Hz^{-1/2}$ due to the elastic structure design with ultra-low elastic coefficient. However, the improvement of sensitivity is achieved by reducing the elastic coefficient rather than optical approaches, which inevitably leads to the decline of bandwidth (below 1 or even 0.1 Hz), dynamic range (~*mg* range), and other performances.

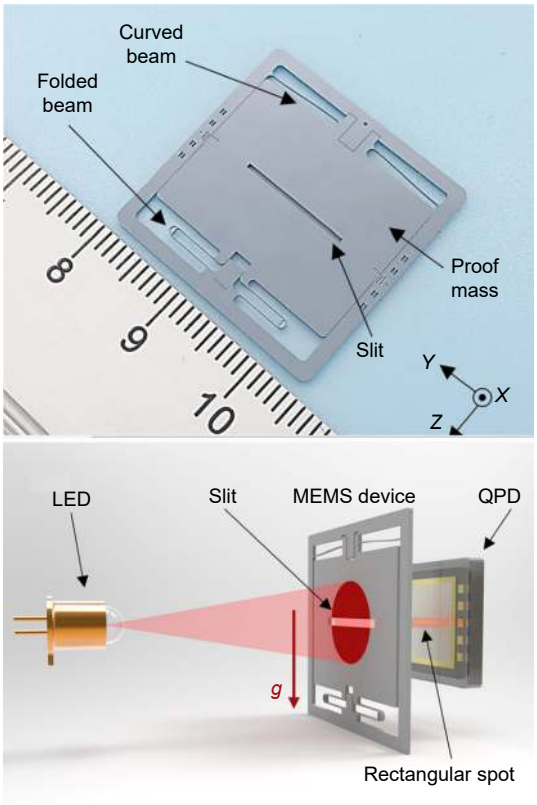

Fig. 7 | Schematic of the MOEMS accelerometer. Figure reproduced with permission from ref.[24], Springer Nature.

To sum up, the MOEMS accelerometers based on geometric optics are capable of achieving simple structure and low cost measurement of acceleration, because no high requirements for light sources and detectors are involved. Nevertheless, the measurement, especially the optical displacement measurement unit, would be significantly affected by the fluctuation of the light source and environmental factors. Thus, this type of MOEMS accelerometer has some limitations in high precision acceleration measurement even though there is some room to modify the mechanical sensing unit.

Wave optics based MOEMS accelerometers

Principle

The optical displacement measurement unit of a wave optics based accelerometer is based on the wave aspect of light. When the accelerometer is subjected to an external

acceleration, the inertia force leads to a displacement of the proof mass, which causes the wavelength (or frequency/phase) change. By detecting the corresponding change, the displacement and the input acceleration can be obtained with relatively higher sensitivity due to the accurate scale of the wavelength compared with the amplitude of light. According to the form and measuring principle of the optical displacement measurement unit, the MOEMS accelerometers of wave optics are subdivided into grating interferometric cavity, FBG, Fabry-Perot cavity and photonic crystal, etc.-based categories.

Grating interferometric cavity scheme

Regarding the grating interferometric cavity based accelerometers, the core sensing unit is a cavity of grating interferometer. It is a kind of micro cavity that is composed of a movable diffraction grating (or grating light valve). The variation of the cavity length changes the intensity of the emitted light by modulating the optical path difference. Taking the wavelength as the ruler, the grating interferometric cavity is able to achieve the sub-nanometer scale precision, thus, paves the way for the higher precision acceleration measurement. Moreover, this type of MOEMS accelerometer has compact optical path and setup, so it also has advantages in miniaturization and integration.

At the end of last century, Cooper et al.[29] built the first accelerometer based on grating light value in light of the probe displacement measuring mechanism of an atomic force microscopes. The schematic diagram is shown in Fig. 8(a). The movable interdigital fingers on the proof mass and the fixed interdigital fingers on the silicon frame constitute a grating light valve. The incident laser beam strikes the grating light valve vertically, and the input acceleration drives the proof mass to have an out-of-plane displacement. The displacement of the movable interdigital fingers, which are fixed on the mass, changes the output light intensity of the interference diffraction beams of the grating light valve. The displacement and the acceleration can be calculated by detecting the output light intensity. This MOEMS accelerometer has a resonant frequency of 906 Hz and a noise equivalent acceleration (NEA) of less than 2 $\mu g \cdot \mathrm{Hz}^{-1/2}$, which outperforms most of its previously reported geometric optics based accelerometers. However, neither the mechanical sensing unit was modified nor other factors were considered such as the parallelism and cross-axis sensitivity. Based upon it, Loh et al.[30] modified the mechanical acceleration sensing structure, as shown in Fig. 8(b) by designing a crab leg-shaped beam-mass structure. This improved the sensitivity and reduced the cross-axis sensitivity of the MOEMS accelerometer. The measured NEA can reach down to 40 $ng \cdot \mathrm{Hz}^{-1/2}$. However, its proof mass center of gravity does not coincide with the beam plane, so that the cross-axis sensitivity is still large. Moreover, the technology maturity is not high due to the lack of packaging and back-end design.

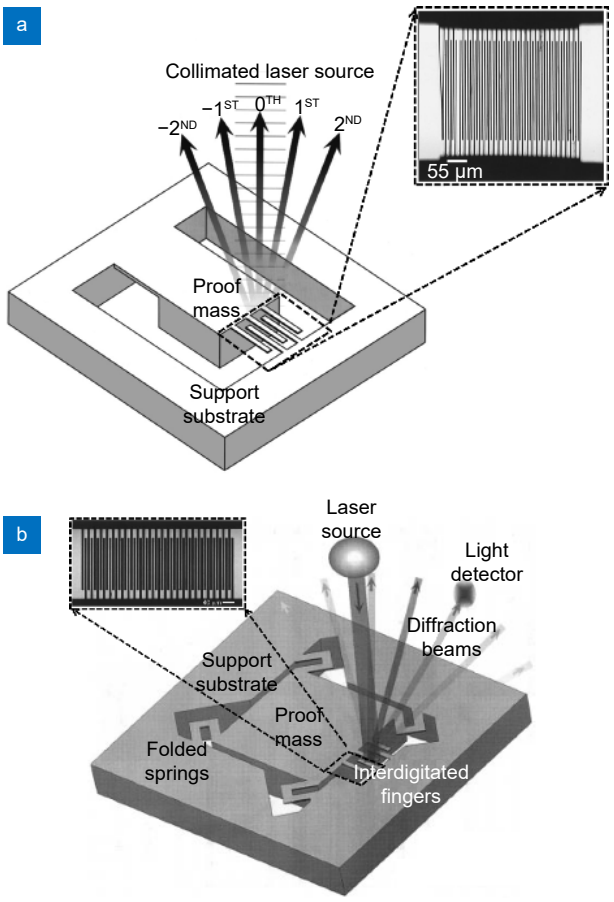

Fig. 8 | (**a**) Simplified model of a MOEMS accelerometer based on grating light valves. (**b**) Another MOEMS accelerometer based on grating light valve. Figure reproduced with permission from: (a) ref.[29], AIP Publishing; (b) ref.[48], IEEE.

Hall et al.[31] made further improvements to the grating light value based MOEMS accelerometers. As shown in Fig. 9, a compact grating interferometric cavity comprising a diffraction grating and a reflective film on the proof mass replaces the grating light valve, so that the reliability and stability of both optical and mechanical units are enhanced. In addition, the accelerometer integrates the electrostatic force feedback electrodes, which can not only maintain working in the position with maximum sensitivity, but can also adjust the mechanical

performances by Q-control. This accelerometer has a thermal-mechanical noise level of 43.7 $ng \cdot Hz^{-1/2}$, and the cross-axis sensitivity is also diminished by modification of the mechanical structure. On this basis, the authors further designed a phase-modulated diffraction grating[32], shown in Fig. 10, to eliminate the zeroth-order reflections of the grating interferometric cavity, and increased the energy efficiency of the signal from less than 30% to around 80%, thus, finally improved the sensitivity of the MOEMS accelerometer. Later in 2016, commercial products of grating interferometric cavity based accelerometer came out. The seismometer developed by Silicon Audio is oriented for geophysical applications, which is able to achieve the sensitivity of less than 1 $ng \cdot Hz^{-1/2}$, while other performances such as dynamic range and bandwidth are acceptable as well.

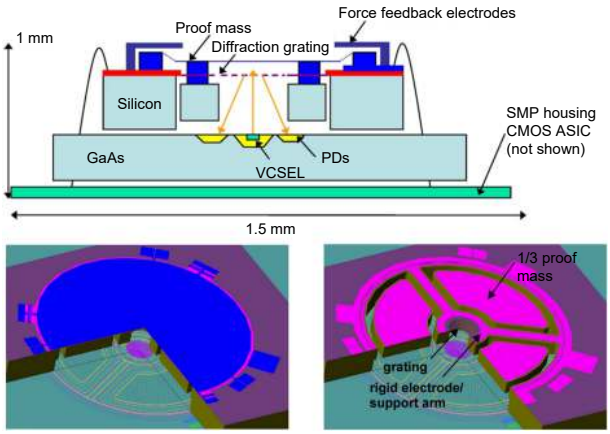

Fig. 9 | Schematic of the grating interferometric cavity based accelerometer. Figure reproduced from ref.[31], IEEE

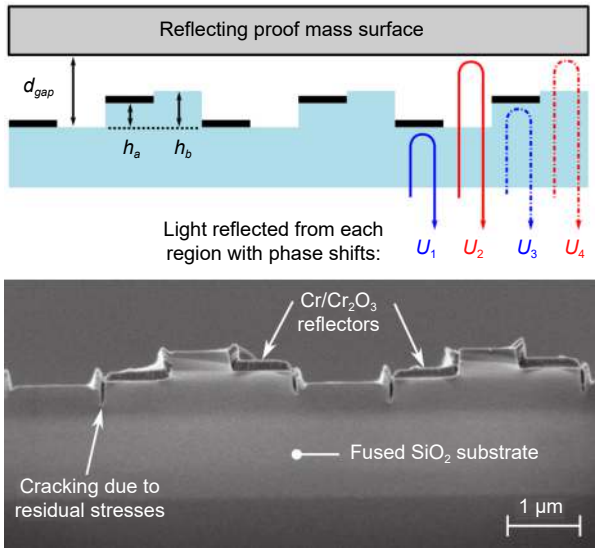

Fig. 10 | A modified phase-modulated grating. Figure reproduced with permission from ref.[32], AIP Publishing.

At the same time, the grating interferometric cavity based accelerometer also derived a lot of improved demonstrations. The measuring principle improving schemes include advanced higher interference diffraction order scheme[33–35], phase modulation and demodulation scheme[36–39], closed-loop feedback scheme[40–42], compensation scheme[39,43], etc. whereas the sensing structure improving schemes include different structural designs[44,45] and different material designs[46], which are all presented in Fig. 11.

In summary, the grating interferometric cavity based accelerometer is one type of the accelerometers based on the wave aspect of light. They were born at the end of last century and developed at the beginning of this century. The technology maturity and performances have been exceedingly improved over the past two decades. By optimizing the structure, introducing phase modulation and various subdivision means, the NEA of interferometric cavity based accelerometers can universally break through 1 $\mu g \cdot Hz^{-1/2}$, and in some cases can reach below 100 $ng \cdot Hz^{-1/2}$. In addition, the cavity based optical displacement measurement unit can be easily integrated with the mechanical sensing structure, bringing the advantages of small size and high stability. In the future, this type of MOEMS accelerometer will be developing towards higher precision, smaller size and stronger environmental adaptability through deep light field manipulation and further optimization of structural and material design in light of different application requirements. However, the further reduction of the size of the optical cavity will lead to the prominent problem of nanoscale effect. In order to approach or exceed the SQL, the development of this type of MOEMS accelerometers is bound to go beyond the scope of the grating interferometric cavity.

Fiber Bragg grating scheme

The optical displacement measurement unit of the FBG based accelerometers is, namely, a Fiber Bragg Grating. When an external acceleration is applied, the inertia displacement of the proof mass produces the strain of the FBG, and changes the wavelength of the output light under the effect of strain. By detecting the wavelength variation, the acceleration can be obtained. FBG based accelerometer is a kind of MOEMS accelerometers which is widely studied and applied extensively at present because of its unique advantages such as good ductility and

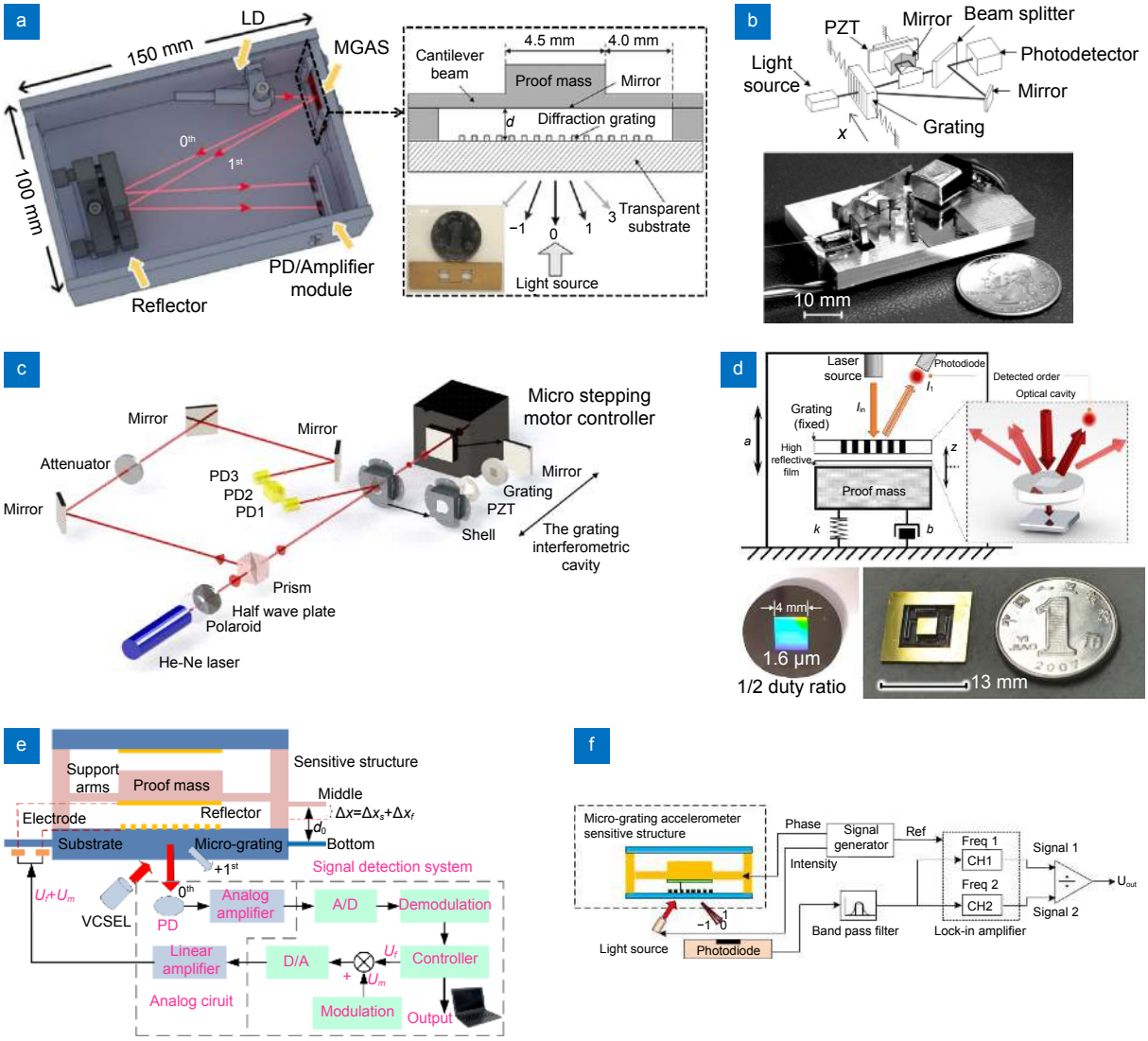

Fig. 11 | (**a**) Differential detection method. (**b**) Another differential detection scheme. (**c**) Compensation scheme. (**d**) High symmetry design. (**e**) Closed-loop feedback scheme. (**f**) Modulation and demodulation scheme. Figure reproduced with permission from: (a) ref.[33], (b) ref.[34], (c) ref.[39] and (f) ref.[36], Optical Society of America; (d) ref.[45], (e) ref.[40], IEEE.

multi-point measurement ability. The measurement principle, performances, advantages and disadvantages of several kinds of FBG based accelerometers are reviewed below.

In 1996, Kersey et al.[47] reported an original FBG based accelerometer. The schematic diagram is shown in Fig. 12, in which the FBG is arranged on an elastic structure made of compliant materials. The external acceleration deforms the elastic structure, and then changes reflected wavelength of the FBG, which is detected by interferometric method. This accelerometer has the sensitivity of 1 $ng \cdot Hz^{-1/2}$ and a bandwidth of 2 kHz. Although it is of relatively low sensitivity and is vulnerable to environmental influences, its advantages of the simplicity, low cost and multi-point measurement ability lead researchers' efforts in the development of this type of MOEMS accelerometer.

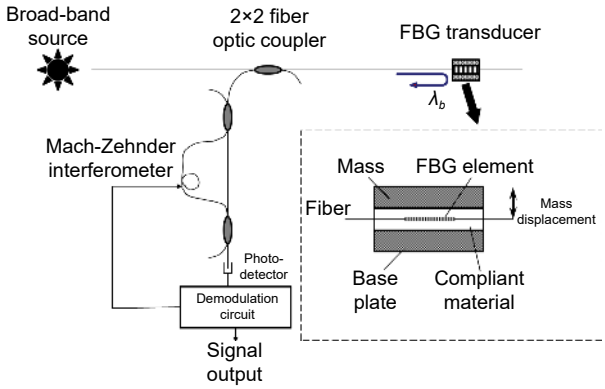

Fig. 12 | Simplified model of an FBG based accelerometer. Figure reproduced with permission from ref.[47], IEEE.

FBG based accelerometer is a good candidate for the building and infrastructure monitoring due to its capability of multi-point measurement. For example, Linze et al.[48] proposed a multi-point FBG based accelerometer, as shown in Fig. 13(a). When subjected to an external acceleration, the mechanical transducers induce birefringence variations within the fiber and in turn change the polarization state, which appears as a power variation as a result. The FBGs reflect light from different positions of the fiber, thus, enabling the wavelength multiplexing. Such setup is able to provide sub-micrometer displacement resolution and excellent sensitivity under the premise of the multi-point measurement function[49]. Researchers also had some attempts to make the FBG accelerometers compatible in the monitoring applications. Mita et al.[50] proposed an FBG based accelerometer in 2001, as shown in Fig. 13(b). The accelerometer is composed of an L-shaped rigid cantilever beam, a proof mass, a spring and a Bragg grating element. The Bragg grating element is not directly attached to the cantilever but is placed onto the cantilever to avoid the uneven strain. Similar design could be found in Guo's[51] report for seismic measurement. The advantage is that the cross-axis sensitivity is small, and the mechanical design ensures a uniform strain distribution of FBG, thus maintaining a good sensitivity over a large amplitude range. However, this design sacrifices the lifetime compared with other demonstrations of the same type. Similarly, Antunes et al.[4] have proposed a modified FBG based accelerometer for the same application. The use of a square-shaped leaf spring minimizes the cross-axis sensitivity and has a balance of the dynamic range and sensitivity. Khijwania's[52] design of a small all-optical FBG based accelerometer, in which the vibration of the sensor replaces the inertia displacement of the proof mass, showing a good vibration monitoring performance.

FBG based accelerometers[53–60] are also suitable for the tilt angle measurement, which is an application of continuing interest in the field of aviation and civil engineering due to its advantages of being inherently self-referencing and the capability in multiplexing, electrically free operation, immunity to radio frequency interference (RFI), and compact size, etc.

Most recently, more attention has been paid to improve the performances of FBG based accelerometers. Obviously, sensitivity is an important parameter for the FBG based accelerometers, so that many attempts and

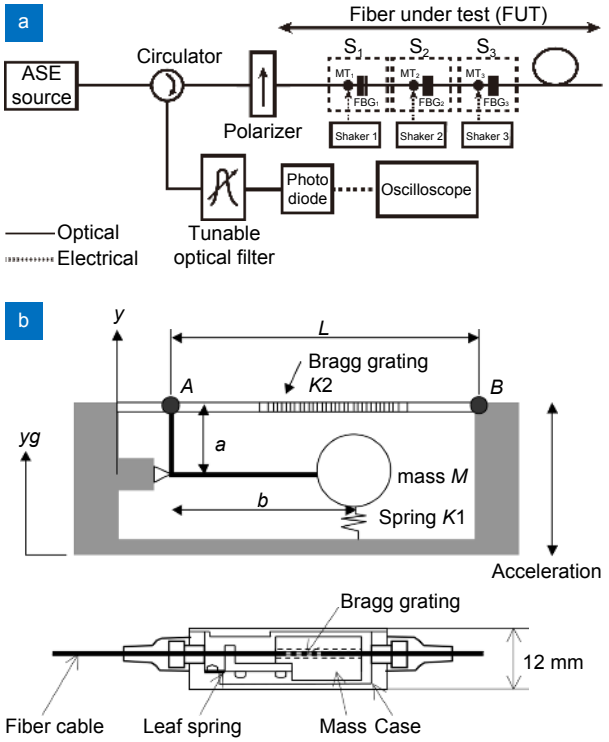

Fig. 13 | (**a**) Schematic of a multi-point FBG based accelerometer. (**b**) Simplified model and physical picture of an FBG based accelerometer. Figure reproduced from: (a) ref.[48], Optical Society of America; (b) ref.[50], SPIE.

theoretical studies have been made to improve it[61–63]. Researchers make their efforts from both the perspective of interior design of fiber, and external setup or mechanical design.

Regarding the design of fiber, Tilted Fiber Bragg Grating (TFBG) is a special FBG to be pointed out, which can efficiently couple the light between the core mode and cladding modes[64–70]. In 2009, Guo et al.[5] proposed a scheme based on TFBG. As shown in Fig. 14(a), it has a taper structure for core mode and cladding. By connecting the modes of core and cladding with taper, it is able to extract the fluctuation of the reflected power of the low-order cladding mode caused by bending, which is proportional to the external acceleration. This characteristic enables the self-calibration function of the accelerometer. The dynamic range of the accelerometer is 0.5–12.5 *g*, and the resonant frequency is adjustable, while the typical value is 51 Hz. The greatest advantage of the accelerometer lies in that the fiber does not need to be stretched, but is embedded into the solid substrate, which maintains a long-term reliability and small size. On the basis of it, Helan et al.[71] optimized the tilt angle of TFBG, as shown in Fig. 14(b), which achieves the maximum ghost peak reflectance. Such type of sensing unit

can be applied to vibration[72] and bending measurement[73], as well as the inclinometer[74].

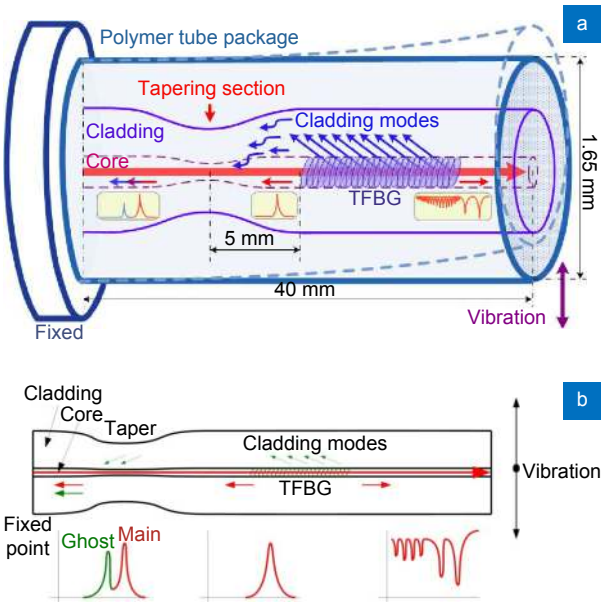

Fig. 14 | (**a**) A compact TFBG based accelerometer. (**b**) Another TFBG based accelerometer. Figure reproduced from: (a) ref.[5] (b) ref.[71], Optical Society of America.

Some others used novel mechanical design to increase the sensitivity of FBG based accelerometers[75]. As shown in Fig. 15, this design adds a buffer layer to increase the distance between the central axis of the cantilever beam and the Bragg grating, and in turn enhances the sensitivity which is proportional to the distance. The additional buffer layer has no influence on the natural frequency of the structure and the strain transferred from the cantilever to the FBG. It has the advantages of simple structure, improved sensitivity without compromising on the bandwidth and other characteristics[76].

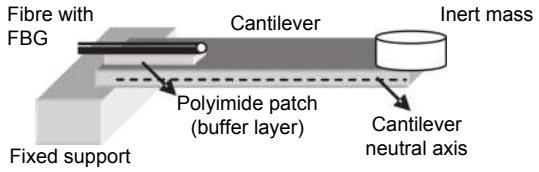

Fig. 15 | An FBG based accelerometer with an additional buffer layer. Figure reproduced with permission from ref.[75], Elsevier.

Birefringence splitting of FBG reflection peak mainly contributed by fiber embedding should be avoided because it would degrade the performance of the optical readout, and further the accelerometer. There are a lot of attempts in order to address this issue[63,77–81]. For example, Todd et al.[82] designed a no-fiber embedded scheme, as shown in Fig. 16(a). The proof mass is welded sandwiched between two parallel plates, and the FBG is attached to the bottom surface of the lower plate. The displacement of the proof mass driven by the acceleration deforms the bottom FBG. The wavelength shift can be obtained by both Fabry-Perot and interferometric means. The unembedded design, shown in Fig. 16, reduces the possibility of birefringence splitting of the FBG reflection peaks and transverse strain-induced. Someone also designed an FBG based accelerometer to eliminate the multi-peak phenomenon by using two sub-beams and a proof mass. Two ends of FBG were stuck between the beam and the cushion block, so as to improve the resistance and sensitivity of transverse interference.

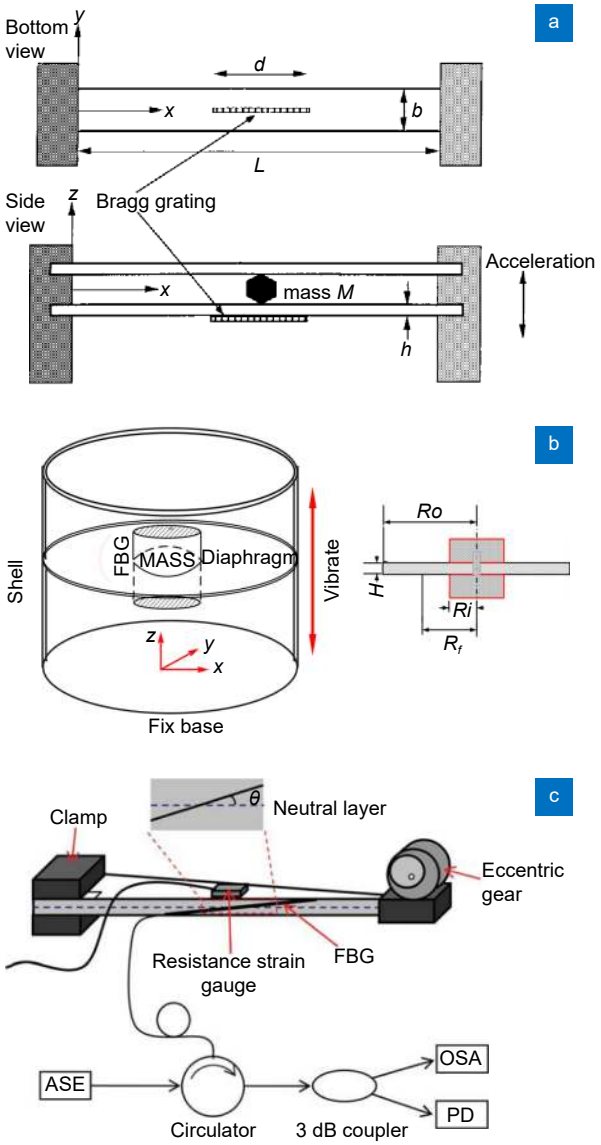

Fig. 16 | (**a**) Simplified model of an optical fiber unembedded FBG based accelerometer. (**b**) Schematic of an optical fiber unembedded FBG based accelerometer. (**c**) An optical fiber unembedded FBG based accelerometer. Figure reproduced with permission from: (a) ref.[82] and (b) ref.[78], IEEE; (c) ref.[81], John Wiley and Sons.

Weight is another factor to consider in the applications of FBG based accelerometers. In 2018, Galv et al.[83] developed a low-weight accelerometer for structural health monitoring in the field of aerospace by combining the FBG and Additive Manufacturing (AM) processes. As shown in Fig. 17, the accelerometer is based on a compliant cylinder with a mass placed on the top and supported by a linear spring fitted with FBG. The inertia displacement of the proof mass under the application of an external acceleration drives the FBG to produce axial strain, and changes the output wavelength. The accelerometer has the sensitivity of 19.65 pm/*g* and a bandwidth of 500 Hz. It can be used extensively for a variety of practical applications due to the advantages of small damping, sufficient rigidity, light weight and high resolution. However, the cross-axis sensitivity is still large. Similarly, Li et al.[84] proposed a micro FBG based accelerometer, in which the length of the vibration arm is only 7 mm. The modified structure helps reduce the size of this accelerometer, overcoming the tradeoff between the sensitivity and resonant frequency. Wei et al.[85] also proposed a miniature FBG vibration sensor, shown in Fig. 18, whose elastic structure is composed of a hinge and an elastic plate. This brings together the advantages of both miniaturization of the sensor and suppressing lateral interference, and the total mass is only 5 *g*.

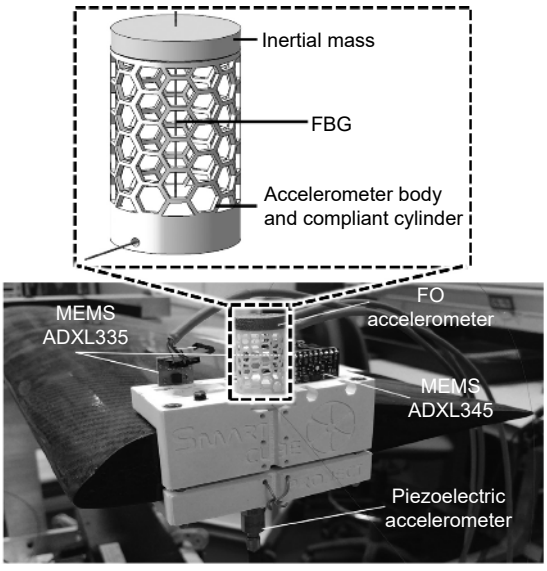

Fig. 17 | A light-weight FBG based accelerometer. Figure reproduced with permission from ref.[83], Elsevier.

In general, the FBG based accelerometers measure the stress, strain, and thus the acceleration through the variation of the Bragg wavelength. This type of MOEMS accelerometer has received the most extensive attention

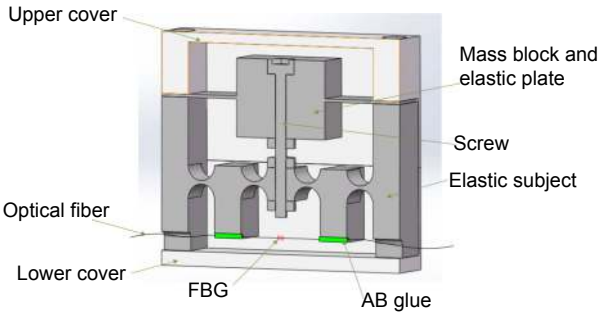

Fig. 18 | A miniature FBG vibration sensor. Figure reproduced with permission from ref.[85], IEEE

over the past 30 years, and extends its application from the basic single-point acceleration measurement to the practical use such as building health monitoring. Regarding the performances, the sensitivity is pushed forward from the NEA of around $mg \cdot \mathrm{Hz}^{-1/2}$ to $\mu g \cdot \mathrm{Hz}^{-1/2}$ level.

The advantages of resistance to electromagnetic interference, low loss, good extension, small volume, and light weight enable the applications of FBG based accelarometer in the complex environment. In addition, the multiplexed FBG based accelerometers provide an effective solution for the implementation in large infrastructures. However, FBG is vulnerable to the influence of ambient temperature and is difficult to compensate. Furthermore, the detection of the wavelength usually requires a complicated readout, which makes the integration difficult.

Fabry-Perot cavity scheme

Fabry-Perot cavity is another candidate of optical displacement measurement unit for a MOEMS accelerometer. As it is subject to acceleration, the inertial force of the proof mass drives the end face of the cavity, changing the reflection or transmission spectrum. By analyzing the spectrum, the magnitude of the input acceleration can be obtained. For MOEMS accelerometers, fiber is always employed to construct a compact Fabry-Perot cavity because its end surface is a natural candidate for a component of the cavity. Herein we review several types of Fabry-Perot cavity based accelerometers, including their principles and performances.

Figure 19 shows an early demonstration of the Fabry-Perot cavity based accelerometer, which is proposed by Gerges[86] in 1989. The accelerometer is composed of two identical hemispherical Fabry-Perot interferometers. Two identical spherical metal mirrors attached to the diaphragm at center, one on each side, forming the outer mirrors of the interferometers, while the distal ends of the fiber serve as the inner mirrors. The variation of the

optical phase is proportional to the applied axial acceleration within the elastic limit of the structure. Setup of two identical interferometers enables common mode suppression, which is able to eliminate the side effects of temperature, environment and cross-coupling. This early accelerometer has an ideal sensitivity of 2.2×10^{-7} $g\cdot \mathrm{Hz}^{-1/2}$ and a resonant frequency of 450 Hz. It is noted that even early demonstration of Fabry-Perot cavity scheme can achieve ultra-high sensitivity ($\mathrm{ng}\cdot \mathrm{Hz}^{-1/2}$ level) by using lock-in or other techniques[87] but with trade-offs on some other performances (for example, bandwidth < 40 Hz).

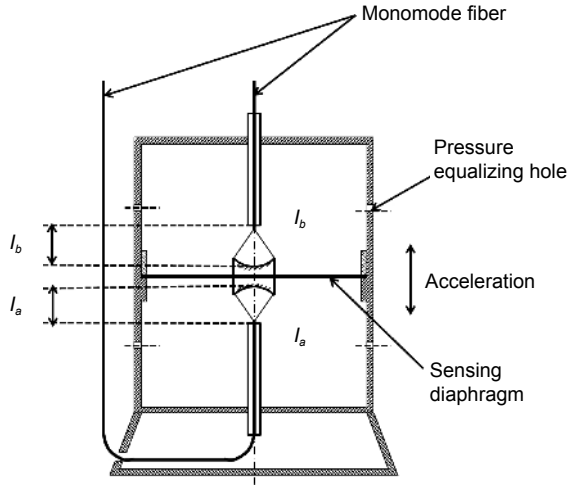

Fig. 19 | Schematic of a Fabry-Perot cavity based accelerometer head. Figure reproduced with permission from ref.[86], Optical Society of America.

In recent years, many attempts have been made to further improve the sensitivity without compromising other performances by means of mechanical design[88–91] or modification of the Fabry-Perot cavity[92–95].

Mechanical amplification is an effective way to improve the sensitivity. For example, Davies et al.[96] introduced a V-beam structure prior to transduction to amplify the displacement of the proof mass. As shown in Fig. 20, the Fabry-Perot cavity comprises the gold-coated silicon block in the middle of the V-beam and at the end surface of a cleaved optical fiber, which acts as both the input and output mirrors. The inertia displacement of the proof mass makes the V-shaped structure compress along the x direction and expand in the y direction, modulating the Fabry-Perot cavity length, which thus changes the wavelength of the output light. The accelerometer has a bandwidth of approximately 10 kHz and a maximum mechanical magnification of 18.6. The use of a V-shaped beam allows the sensitivity enhancement without compromising the bandwidth. Moreover, the displacement as well as the acceleration measurement sensitivity are mechanically adjustable. However, the structure is unstable and the dynamic range is limited. Utilizing a high-speed white light interferometry (WLI) demodulation algorithm to achieve the Fabry-Perot cavity interrogation is another way to improve the sensitivity. Zhao et al.[97] proposed a fiber optic Fabry-Perot accelerometer with WLI, using fast full-spectrum WLI demodulation scheme, the sensing system can achieve high dynamic range, high precision, and high speed simultaneously.

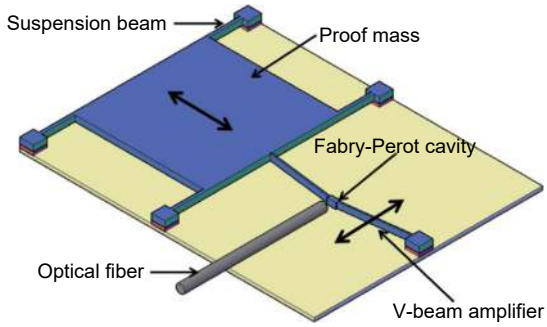

Fig. 20 | Schematic of a V-beam amplified Fabry-Perot cavity based accelerometer. Figure reproduced with permission from ref.[96], Elsevier.

Cavity optomechanics[98–102] has attracted increasing research interest for both fundamental studies and practical applications, and this paves the way for highly sensitive Fabry-Perot cavity based accelerometers. Cervantes et al.[103] presented a modified Fabry-Perot cavity based accelerometer that combines a monolithic fused quartz oscillator and a fiber micro-cavity together, in which the oscillator is of low-loss and compatible with optical cavity. This type of accelerometer can reach a sensitivity of 100 $\mathrm{ng}\cdot \mathrm{Hz}^{-1/2}$. The length determination of similar demonstrations[104,105] enables traceability to the International System of Units, and can obtain high sensitivity as well as a large bandwidth simultaneously at room temperature, while the tradeoff is the increased complexity. Several simple means such as employing a 45-degree mirror in a cavity[106,107] can improve the sensitivity of the system by increasing optical light path without affecting the resonant frequency[108].

There are expensive efforts put in improving other performances apart from the sensitivity. Someone tried to perform multi-axis detection in one accelerometer[109–112,127]. As for the Fabry-Perot cavity based

accelerometer, in 2011 Lin et al.[90] designed a multi-axis accelerometer by arranging the three headers orthogonally, as shown in Fig. 21. The inertia displacement of the proof mass is detected by a micro-mirror installed in the center of it, and a fiber cracked at the end is fixed in the V-groove to ensure the surface is parallel to the micro-mirror, forming a Fabry-Perot cavity. The accelerometer has the sensitivity of 48 $ng \cdot Hz^{-1/2}$, a bandwidth of 160 Hz, along with the advantage of multi-directional measurement.

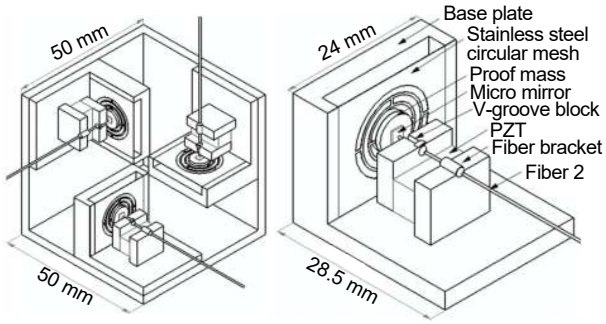

Fig. 21 | Structure of a multidirectional Fabry-Perot cavity based accelerometer. Figure reproduced with permission from ref.[113], IOP Publishing.

Other researchers tried to combine the optical fiber with the Fabry-Perot cavity to construct high multifunctional sensors, which are capable of detecting a wide range of physical parameters such as dynamic strain[113–116], temperature[114–119], vibration[120–123], pressure[124,125], and refractive index[119,126]. Also, some attempts have been made to measure acceleration[128–130], whilst several demonstrations are represented in Fig.22. Jia et al.[130] presented an active temperature-compensated fiber Fabry-Perot accelerometer that can measure vibration and temperature simultaneously. By attaching all silicon in-line fiber Fabry-Perot etalon to a surface of triangular cantilever and attaching mass blocks at the free end for vibration measurement, a proportional-integral-derivative (PID) algorithm of temperature compensation is used for feedback control of laser wavelength to realize synchronous measurement of acceleration and temperature. Zhu et al.[120]proposed an all-fiber vibration sensor based on the fiber Fabry-Perot interferometer, in which the optical fibers are chemically etched into cantilever beams and proof mass, and further protected by a quartz tube to ensure the sensor can be adapted to different practical requirements.

In recent decades, Fabry-Perot cavity based accelerometers have gained increased attention due to their high sensitivity, compact structure, and simple optical path. The theoretical performances of the Fabry-Perot cavity based accelerometer could be very high, for example, the improvednoiseequivalentdisplacementoftheopticaldisplacement sensing unit can reach as low as 10^{-14} $m \cdot Hz^{-1/2}$, and the corresponding acceleration measurement sensitivity is sub-μg level. The performance and form are flexible and adjustable[113,131–137] according to different application requirements. However, it requires high micromachining precision, and may suffer from poor repeatability

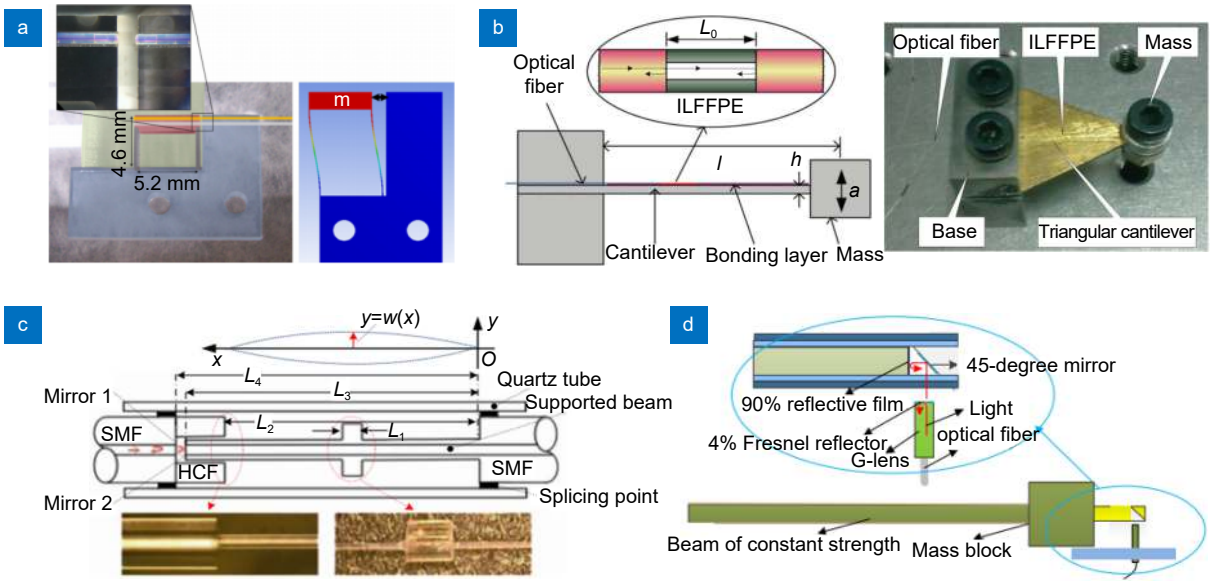

Fig. 22 | (**a**) Photograph and sketch of a Fabry-Perot accelerometer. (**b**) Structural configuration and photograph of a Fabry-Perot cavity based accelerometer. (**c**) Simplified model of an all-optical fiber vibration sensor. (**d**) A 45° Fabry-Perot interferometric cavity based accelerometer. Figures reproduced with permission from: (a) ref.[103], AIP Publishing; (b) ref.[130], IEEE; (c) ref.[120], Optical Society of America; (d) ref.[108], SPIE.

and dynamic range due to the limited cavity length.

Photonic crystal scheme

For photonic crystal based accelerometers, the optical displacement sensing measurement unit is usually a one- or two-dimensional photonic crystal waveguide. Photonic crystals have photonic band gap, which has a selectivity for the wavelength of the light propagating in. The external acceleration deforms the periodic photonic structure, thus breaking and changing the selectivity. The acceleration is obtained by detecting the variation of wavelength (or other properties of light). Photonic crystal accelerometers usually have a large bandwidth due to their high Q value, and they also have high device compactness. Herein we present the principles, properties, advantages and disadvantages of several typical demonstrations of photonic crystal based accelerometers.

In 2004, Jaksic et al.[138] proposed a MOEMS accelerometer based on a photonic crystal waveguide containing defects coated on a diaphragm, as shown in Fig. 23. Two defects are embedded in the photonic crystal structure, in which only a single local mode is allowed to propagate. The local mode of two defects is the same and the transmission through the waveguide is the largest in absence of external acceleration, while the external acceleration will change the local mode of the defects, causing the transmission peak mismatch and transmission intensity reduction. This early photonic crystal based accelerometer shows the advantages of simple manufacturing, all-optical signal communication, and high chip integration, but the precision is not high and the performance is subjected to the experimental factors.

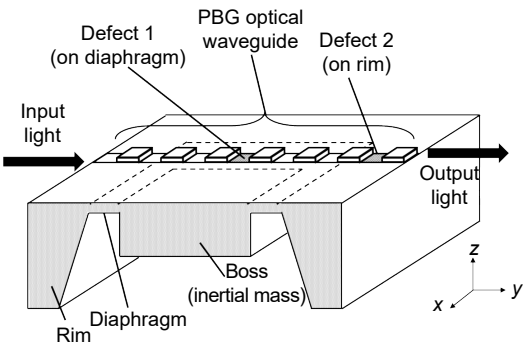

Fig. 23 | An early demonstration of MOEMS accelerometer based on photonic crystal. Figure reproduced with permission from ref.[138], IEEE.

Photonic crystal structures include one-[139,140] and two-dimensional[141] photonic crystals, which can both be used as the optical sensing unit. Typical one-dimensional photonic crystal based accelerometer is shown in Fig. 24[142]. The optical sensing unit, a one-dimensional photonic crystal, consists of alternating silicon and air. When there is an external acceleration, the interdigital silicon fingers attached to the proof mass move along the sensing direction, changing the periodicity condition, which alters the central wavelength of the output mode. The advantages are that the accelerometer has linear response to the applied acceleration in the whole measurement range, low cross-axis sensitivity, high reliability and integration.

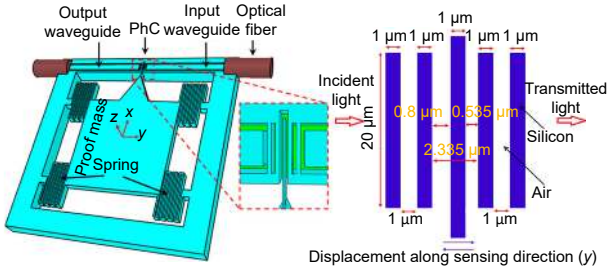

Fig. 24 | 3D model of a photonic crystal based accelerometer. Figure reproduced with permission from ref.[142], IEEE.

The same author also designed a two-dimensional photonic crystal accelerometer based on wavelength modulation[141]. This scheme consists of a laser diode light source, an adjustable Add-Drop filters (ADF) based on the principle of ring resonator (RR), photoelectric detector and an integrated waveguide. The coupled light with wavelengths meeting the RR conditions, is propagating into the RR and is then coupled into the drop waveguide. As shown in Fig. 25, while an external acceleration is applied, the displacement makes the radius of the RR larger, which leads to a redshift of the wavelength of the output resonance mode. Both amplitude and direction of the acceleration can be interpreted by detecting the wavelength shifts in the readout system.

Currently, the research about photonic crystal based accelerometers is gaining rising attention and rapid development[143]. This kind of accelerometer usually has a high Q value, along with the reasonable sensitivity and bandwidth. How to improve the environmental stability and enhance the repeatability (both in performance and fabrication process) is the development priority of this kind of MOEMS accelerometer, and it is also the route to the practical application. In addition, Maybe the future trend of photonic crystal accelerometers is to combine with other elements, such as near field.

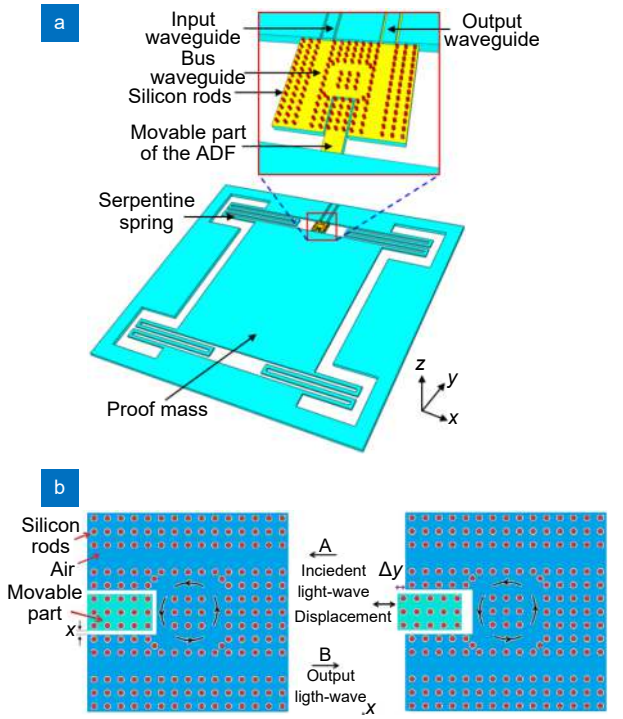

Fig. 25 | (**a**) Simplified model of a photonic crystal accelerometer along with (**b**) the working principle of ADF. Figure reproduced with permission from: (a, b) ref.[141], IEEE.

Summary of wave optics based accelerometers

As mentioned earlier, MOEMS accelerometers based on the principle of wave optics can generally improve the performances, especially the sensitivity, when compared to the geometric optics based accelerometers. They can be well adapted to different applications due to the various forms. Among them, the grating interferometric cavity based accelerometer is a MOEMS accelerometer with a relatively high precision, and the NEA can easily reach down to 100 $ng \cdot Hz^{-1/2}$ or even lower. FBG based accelerometer is the most widely studied and used accelerometer. Its unique high ductility enables applications in building monitoring and other fields, but it has slightly mediocre performance in sensitivity. Fabry-Perot cavity and photonic crystal based accelerometers feature higher sensitivity. Correspondingly, they have higher requirements for micro-machining precision, the maturity of which still needs to be improved. Wave optics based MOEMS accelerometers are gradually approaching the SQL, which cannot be broken through by the standard scalar diffraction theory because of the approximations and assumptions involved in. However, this big class of MOEMS accelerometer still has good technical advancements and scene adaptivity to many applications, and therefore still has a large room for development.

New optomechanical accelerometer

Aforementioned MOEMS accelerometers based on geometric optics and wave optics have relatively high precisions, large dynamic ranges, as well as electrical insulating properties due to the advantages of the optical displacement measurement unit, and can be applied to many application scenes. However, regarding the propagation characteristics of light, these two kinds of MOEMS accelerometers both make approximations to some degrees, which not only provide an inaccurate interpretation of the nanoscale optical effects, but also lose the high-frequency information in the near-field. In order to break through the sensitivity limit of the MOEMS accelerometer, for example, approaching or even exceeding the SQL, researchers experimented with light field manipulation in scale of sub-wavelength and utilization of light-matter interaction, to push the sensitivity beyond the state of the art.

Taking advantages of surface plasmon[144,145] is an effective means to break through the sensitivity limit because it is able to extract the near-field information which is dissipated in the far-field optics. Surface plasmon can be realized in principle by coupling the evanescent waves through a prism, by nano-fabricated metastructures[146], or by bringing a close nano-sized light source, whereas the nano-fabricated structure is more feasible for accelerometers. Early in 2003, Carr et al.[147] from Sandia laboratory designed a sub-wavelength displacement sensing structure based on coupling of surface plasmons, which comprises a period-reduced silicon grating pair and an absorption layer made of silicon nitride. This structure was proved to have an equivalent noise displacement of $fm{\cdot}Hz^{-1/2}$ level. On the basis of the displacement sensing structure, the authors constructed a near-field MOEMS accelerometer in conjunction with the serpentine beams and electrostatic actuation[148,149], as shown in Fig. 26, which achieves an NEA of 17 $ng \cdot Hz^{-1/2}$ and a mechanical-thermal noise level of 8 $ng \cdot Hz^{-1/2}$. Extremely high sensitivity and small size make it a compelling device that holds the promise of applications in molecular force detection, friction dynamics and other fields, whereas the large-scale application of this MOEMS accelerometer is stymied by the relatively complex structure and micromachining process.

In 2012, Painter et al.[150] designed another type of surface plasmon based accelerometer, in which a zipper photonic-crystal nanocavity serves as the superior optical displacement readout of $fm \cdot Hz^{-1/2}$ level, as shown in

Fig. 27. The zipper nanocavity[151,152], shown in Fig. 27(a), enables an imprecision near the SQL, allowing the accelerometer to break through the SQL by using additional high Q-factor mechanical design and strong thermo-optomechanical backaction to damp and cool the thermal motion of the proof mass[153]. The dimensions of the mass and the elastic structure are both in micrometer scale, which enable high integration and dynamic performances. The MOEMS accelerometer can achieve a practical noise equivalent acceleration of 10 $\mu g \cdot \mathrm{Hz}^{-1/2}$ while maintaining a bandwidth of more than 20 kHz and a dynamic range of greater than 40 dB. However, there is still some room for the performance improvement due to the small proof mass and lack of designated optimization of the acceleration sensing structure.

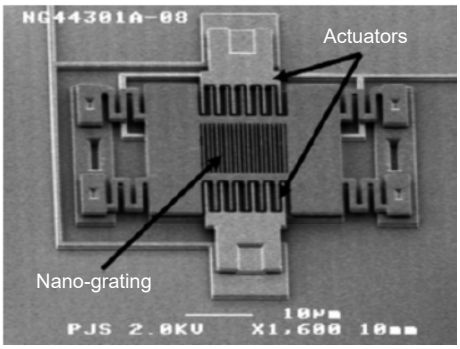

Fig. 26 | SEM of the near-field MOEMS accelerometer based on vertically stacked sub-wavelength nano-gratings. Figure reproduced with permission from ref.[149], Elsevier.

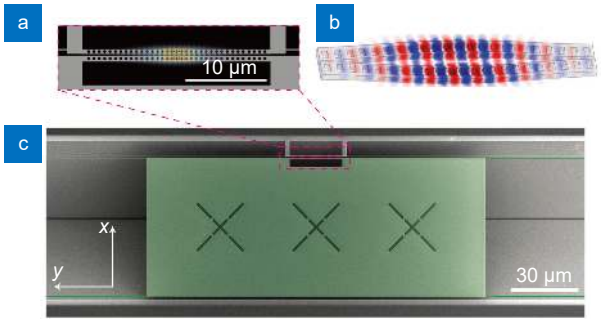

Fig. 27 | (**a**) Zoom-in of the zipper nanocavity region. (**b**) Schematic of the distorted zipper cavity showing the magnitude of the electric field. (**c**) False-coloured SEM image of the typical optomechanical accelerometer. Figure reproduced with permission from ref.[150], Springer Nature.

Other forms of surface plasmon based cavity also proved themselves as potential candidates of ultra-sensitive optical displacement readout with high compactivity. For example, Kim[154], Zobenica[155] and Wong[156] all reported surface plasmon based sensors, shown in Figs. 28(a)–28(c), which have a noise level of fm $\cdot \mathrm{Hz}^{-1/2}$, and further enable functionalities of highly sensitive acceleration (10 $ng \cdot \mathrm{Hz}^{-1/2}$ or even lower), weight and torque detection. But one should take into account that these sensors are still limited in applications in terms of their demanding requirements for working environment (cryogenic or vacuum) and micromachining design and process.

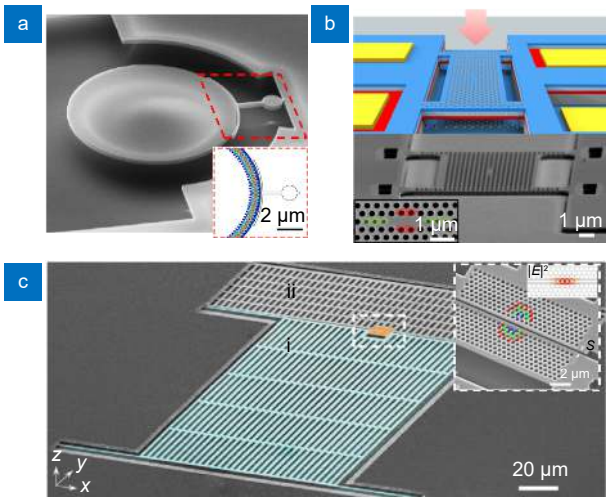

Fig. 28 | (**a**) Scanning electron micrograph along with the finite element model of the optical resonance of the optomechanical sensor (**b**) Sketch of the optomechanical sensor and the zoom-in SEM image showing the active part designed (**c**) A chip-scale optomechanical inertial sensor based on surface plasmon coupling. Figure reproduced with permission from: (a) ref.[154] and (b) ref.[155], Springer Nature; (c) ref.[156], John Wiley and Sons.

There are still several demonstrations of practical MOEMS accelerometers based on surface plasmon coupling by means of nanocavity or nanostructure, such as the designs proposed by Rogers[157], Feng[158], and Lu[159], etc. However, the performance is not perfectly correlated to the physical picture. More specifically, the schemes utilizing the coupling of surface plasmon would have relatively low sensitivity if one just serves the sub-wavelength structure as a diffraction unit. We have to take the consideration of the mechanical design and the transfer function of final output versus input together during the performance estimation of a MOEMS accelerometer.

The light-matter interaction of the optomechanical cavity receives extensive attention over the past decades, and it is the other avenue to realize the ultra-sensitive acceleration measurement, which has been identified as one of the most effective gravity estimation methods[160–162]. Recently, researchers are leading their efforts in the miniaturization of the cavity, thus pushing the light-matter coupling scheme into the region of

compact MOEMS accelerometer.

Underpinned with the quantum investigation of the theoretical effectiveness of measuring acceleration through light-matter interaction[163–165], several typical compact optomechanical cavity forms were performed. As shown in Fig. 29, the matter could be a microdisk[166], an elastic mechanical mirror[164], a nanosphere[165], and the cavity could be ring shaped[167], etc. On the basis of these theories and cavity apparatuses, MOEMS accelerometers feature sub-ng resolution and down to sub-μGal·Hz$^{-1/2}$ noise level, such as Purdy[168] and Abend's[169] demonstrations, shown in Figs. 30(a) and 30(b). The compact ultra-sensitive optomechanical accelerometer has also been successfully employed to practical applications combining with classical accelerometers to obtain a long-period navigation-grade stability[170].

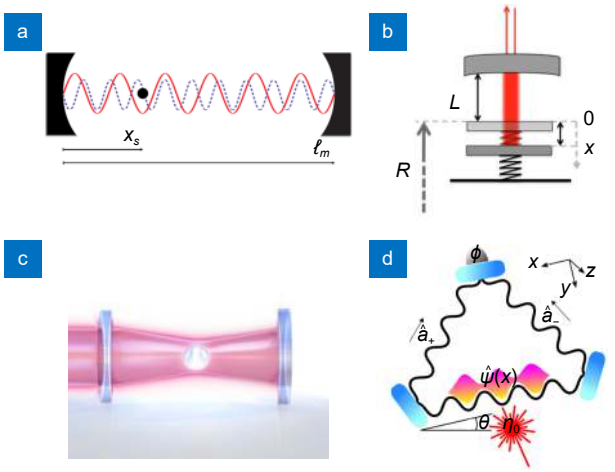

Fig. 29 | Schematics of different setups for light-matter interaction based detection. (**a**) A cavity with a microdisk trapped by a light field, which is cooled for a readout by a second light field[166]. (**b**) An optomechanical cavity with an injected light field and an elastic mechanical mirror[164]. (**c**) An optomechanical system with a trapped and laser-cooled nanodiamond[165]. (**d**) A ring cavity comprising three tilted mirrors[167]. Figure reproduced with permission from: (a) ref.[166] and (b) ref.[164], America Physical Society; (c) ref.[165], Springer Nature; (d) ref.[167], John Wiley and Sons.

The underlying idea of the light-matter interaction, or more specifically, the cavity optomechanics is not the topic of this review. Ones could refer to ref.[102,171] to have a comprehensive understanding of the field and applications. In addition, although gravimetry is a kind of accelerometer, it has a wide extension, and includes a lot of sub-categories, while all of these are not fully discussed in this paper.

To sum up, the research of new optomechanical MOEMS accelerometers has been accelerating rapidly

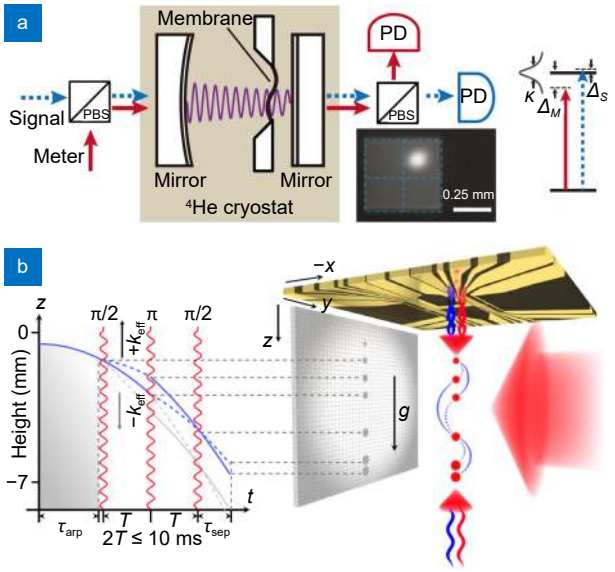

Fig. 30 | (**a**) Experimental setup of the ultra-sensitive optomechanical system proposed. (**b**) An atom-chip based accelerometer setup and space-time trajectories. Figure reproduced with permission from: (a) ref.[168], The American Association for the Advancement of Science; (b) ref.[169], America Physical Society.

since its birth in the new century. This type of MOEMS accelerometer surpasses the limitation of scalar diffraction theory in terms of the measurement principle. By extracting the high frequency information of the near-field or quantum states through the light-matter interaction, the accelerometer is able to approach or exceed the SQL. A variety of new demonstrations are constantly emerging while the researchers pay more attention to the breakthrough of the measurement principle at present and try to draw the physical picture of the nano-scale behind the phenomenon. As a result, the technology maturity is generally not high, and most of the demonstrations remain just a proof-of-principle, which is far from being implemented in applications. In the future, the new optomechanical MOEMS accelerometers will pursue both the innovation of the mechanism and design, as well as the technical feasibility and maturity, which cannot only push forward the theoretical performances, but can also strive to translate the advanced principle to the advanced technology and devices to meet the rising requirements.

Conclusion and prospect

MOEMS accelerometers have progressed significantly since the first demonstration was reported in 1980s. By taking the advantages of both the MEMS and optical sensing technologies, MOEMS accelerometers are now capable of achieving impressive level of performances.

Table 1 | Typical specifications of various MOEMS accelerometers along with their characteristics and applications

Parameter	Geometric optics based	Wave optics based				New optomechanical
		Grating interferometric cavity based	Fiber Bragg grating based	Fabry-Perot cavity based	Photonic crystal	
Optical displacement resolution	μm~nm scale	sub-nm	nm scale	nm~pm scale	sub-nm	up to fm level
Noise equivalent acceleration	$mg{\cdot}Hz^{-1/2}$~$ng{\cdot}Hz^{-1/2}$ (depend on mechanical design)	$\mu g{\cdot}Hz^{-1/2}$~$ng{\cdot}Hz^{-1/2}$	sub-$\mu g{\cdot}Hz^{-1/2}$	$\mu g{\cdot}Hz^{-1/2}$~$ng{\cdot}Hz^{-1/2}$	sub-$\mu g{\cdot}Hz^{-1/2}$	up to sub-$ng{\cdot}Hz^{-1/2}$
Characteristics	Simple structure, low cost, moderate sensitivity	High compactness, high sensitivity	Multi functionality, moderate sensitivity	Flexible form, high sensitivity	High integration, high sensitivity	Ultra-high sensitivity
Scope of applications	Daily applications to geophysical applications	Inertial navigation, geophysical applications	Daily applications, infrastructure monitoring	Inertial navigation, geophysical applications	Inertial navigation	Inertial navigation, geophysical applications

This paper first analyzes practical and potential demands of applications for MOEMS accelerometers, and then roughly divides the accelerometers into three main categories in terms of the optical sensing principle. The performances, especially the sensitivity, are generally increasing from the geometric optics based, to wave optics based, and finally to the new optomechanical accelerometers, as listed in Table 1. However, it should be noted that each category has its own merits and demerits, which are adapted to different requirements. Also, not all applications require extremely high sensitivity or precision. For example, the geometric optics based accelerometers usually have a relatively simple structure and low cost, one can routinely measure m*g* scale accelerations in daily applications by using this type of accelerometer. The wave optics based accelerometers are extensively studied and contain a lot of sub-categories, and some are able to provide μ*g* performance adapted to applications such as inertial navigation, while some specialize in other performances such as multi-point and multi-axis measurement. The new optomechanical accelerometers have been demonstrated to hold the promise of realizing ultra-high sensitivity, which can approach or even being pushed beyond the SQL. However, they are not yet ripe, let alone enter the large-scale application stage.

In the following decades, the community of MOEMS accelerometer will continue to flourish, while much effort would be expended to collaborative design for both optical and mechanical components, improvement of the technological maturity, as well as advance precision micromachining. Researchers will also strive to further develop more reliable accelerometers with higher performances for specific applications including inertial navigation and microgravity measurement, as well as emerging and as yet unknow applications.

References

1. Liu HF. Design, fabrication and characterization of a MEMS gravity gradiometer (Imperial College London, London, 2016).
2. Yazdi Z, Ayazi F, Najafi K. Micromachined inertial sensors. *Proc IEEE* **86**, 1640 (1998).
3. Eloy JC. *Advanced Microsystems for Automotive Applications 2005* (Springer, Berlin, Heidelberg, 2005).
4. da Costa Antunes PF, Lima HFT, Alberto NJ, Rodrigues H, Pinto PMF et al. Optical fiber accelerometer system for structural dynamic monitoring. *IEEE Sens J* **9**, 1347–1354 (2009).
5. Guo T, Shao LY, Tam HY, Krug PA, Albert J. Tilted fiber grating accelerometer incorporating an abrupt biconical taper for cladding to core recoupling. *Opt Express* **17**, 20651 –20660 (2009). DOI: 10.1117/12.851427
6. Wang Q, Liu HF, Tu LC. High-precision MEMS inertial sensors for geophysical applications. *Navig Control* **17**, 1 (2018).
7. Tveten AB, Dandridge A, Davis CM, Giallorenzi TG. Fibre optic accelerometer. *Electron Lett* **16**, 854–856 (1980).
8. Abbaspour-Sani E, Huang RS, Kwok CY. A novel optical accelerometer. *IEEE Electron Device Lett* **16**, 166–168 (1995).
9. Hortschitz W, Kainz A, Kovacs G, Steiner H, Stifter M et al. Robust, ultra sensitive MOEMS inertial sensor read out with infrared light. In *Proceedings of 2018 IEEE Micro Electro Mechanical Systems* 952 –955 (IEEE, 2018); http://doi.org/10.1109/MEMSYS.2018.8346715.
10. Qin Y, Brockett A, Ma Y, Razali A, Zhao J et al. Micro-manufacturing: research, technology outcomes and development issues. *Int J Adv Manuf Technol* **47**, 821–837 (2010).
11. Tilli M, Paulasto-Kröckel M, Petzold M, Theuss H, Motooka T et al. *Handbook of Silicon Based MEMS Materials and Technologies* 3rd ed (Elsevier, Amsterdam, 2020).
12. Lu BH, Lan HB, Liu HZ. Additive manufacturing frontier: 3D printing electronics. *Opto-Electron Adv* **1**, 170004 (2018).
13. Huang YA, Wu H, Xiao L, Duan YQ, Zhu H et al. Assembly and applications of 3D conformal electronics on curvilinear

surfaces. *Mater Horiz* **6**, 642–683 (2019).
14. Dao DV, Nakamura K, Bui TT, Sugiyama S. Micro/nano-mechanical sensors and actuators based on SOI-MEMS technology. *Adv Nat Sci Nanosci Nanotechnol* **1**, 013001 (2010).
15. Zhou GY, Chau FS. Grating-assisted optical microprobing of in-plane and out-of-plane displacements of microelectromechanical devices. *J Microelectromech Syst* **15**, 388–395 (2006).
16. Bramsiepe SG, Loomes D, Middlemiss RP, Paul DJ, Hammond GD. A high stability optical shadow sensor with applications for precision accelerometers. *IEEE Sens J* **18**, 4108–4116 (2018).
17. Plaza JA, Llobera A, Dominguez C, Esteve J, Salinas I et al. BESOI-based integrated optical silicon accelerometer. *J Microelectromech Syst* **13**, 355–364 (2004).
18. Schröpfer G, Elflein W, de Labachelerie M, Porte H, Ballandras S. Lateral optical accelerometer micromachined in (100) silicon with remote readout based on coherence modulation. *Sens Actuat A-Phys* **68**, 344–349 (1998).
19. Cadarso VJ, Llobera A, Villanueva G, Seidemann V, Büttgenbach S et al. Polymer microoptoelectromechanical systems: accelerometers and variable optical attenuators. *Sens Actuat A-Phys* **145**, 147–153 (2008).
20. Llobera A, Seidemann V, Plaza JA, Cadarso VJ, Buttgenbach S. Integrated polymer optical accelerometer. *IEEE Photonics Technol Lett* **17**, 1262–1264 (2005).
21. Llobera A, Seidemann V, Plaza JA, Cadarso VJ, Buttgenbach S. SU-8 optical accelerometers. *J Microelectromech Syst* **16**, 111–121 (2007).
22. Pike WT, Standley IM, Calcutt SB, Mukherjee AG. A broadband silicon microseismometer with 0.25 NG/rtHz performance. In *Proceedings of 2018 IEEE Micro Electro Mechanical Systems (MEMS)* 113–116 (IEEE, 2018); http://doi.org/10.1109/MEMSYS.2018.8346496.
23. Middlemiss RP, Samarelli A, Paul DJ, Hough J, Rowan S et al. Measurement of the Earth tides with a MEMS gravimeter. *Nature* **531**, 614–617 (2016).
24. Tang SH, Liu HF, Yan ST, Xu XC, Wu WJ et al. A high-sensitivity MEMS gravimeter with a large dynamic range. *Microsyst Nanoeng* **5**, 45 (2019).
25. Mustafazade A, Pandit M, Zhao C, Sobreviela G, Du ZJ et al. A vibrating beam MEMS accelerometer for gravity and seismic measurements. *Sci Rep* **10**, 10415 (2020).
26. Duan YX, Wei XY, Wang HR, Zhao MH, Ren ZM et al. Design and numerical performance analysis of a microgravity accelerometer with quasi-zero stiffness. *Smart Mater Struct* **29**, 075018 (2020).
27. Jeong Y, Daruwalla A, Wen H, Ayazi F. An out-of-plane "hinge-shaped" nano-gap accelerometer with high sensitivity and wide bandwidth. In *Proceedings of the 19th International Conference on Solid-State Sensors, Actuators and Microsystems (TRANSDUCERS)* 2131–2134 (IEEE, 2017); http://doi.org/10.1109/TRANSDUCERS.2017.7994496.
28. Zhang HC, Wei XY, Ding YY, Jiang ZD, Ren J. A low noise capacitive MEMS accelerometer with anti-spring structure. *Sens Actuat A-Phys* **296**, 79–86 (2019).
29. Cooper EB, Post ER, Griffith S, Levitan J, Manalis SR et al. High-resolution micromachined interferometric accelerometer. *Appl Phys Lett* **76**, 3316–3318 (2000).
30. Loh NC, Schmidt MA, Manalis SR. Sub-10 cm^3 interferometric accelerometer with nano-g resolution. *J Microelectromech Syst* **11**, 182–187 (2002).
31. Hall NA, Okandan M, Littrell R, Serkland DK, Keeler GA et al. Micromachined accelerometers with optical interferometric read-out and integrated electrostatic actuation. *J Microelectromech Syst* **17**, 37–44 (2008).
32. Williams RP, Hord SK, Hall NA. Optically read displacement detection using phase-modulated diffraction gratings with reduced zeroth-order reflections. *Appl Phys Lett* **110**, 151104 (2017).
33. Wang X, Feng LS, Yao BY, Ren XY. Sensitivity improvement of micro-grating accelerometer based on differential detection method. *Appl Opt* **52**, 4091–4096 (2013).
34. Chen LH, Lin Q, Li S, Wu X. Optical accelerometer based on high-order diffraction beam interference. *Appl Opt* **49**, 2658–2664 (2010).
35. Zhang Y, Gao S, Xiong H, Feng LS. Optical sensitivity enhancement in grating based micromechanical accelerometer by reducing non-parallelism error. *Opt Express* **27**, 6565–6579 (2019).
36. Zhang TH, Liu HL, Feng LS, Wang X, Zhang Y. Noise suppression of a micro-grating accelerometer based on the dual modulation method. *Appl Opt* **56**, 10003–10008 (2017).
37. Zhao SS, Hou CL, Bai J, Yang GG, Tian F. Nanometer-scale displacement sensor based on phase-sensitive diffraction grating. *Appl Opt* **50**, 1413–1416 (2011).
38. Zhao SS, Zhang J, Hou CL, Bai J, Yang GG. Optical accelerometer based on grating interferometer with phase modulation technique. *Appl Opt* **51**, 7005–7010 (2012).
39. Lu QB, Wang C, Bai J, Wang KW, Lian WX et al. Subnanometer resolution displacement sensor based on a grating interferometric cavity with intensity compensation and phase modulation. *Appl Opt* **54**, 4188–4196 (2015).
40. Li H, Li SK, Deng KK, Gao S, Feng LS. Analysis and design of closed-loop detection technique for micro-grating accelerometer. *J Lightwave Technol* **36**, 5738–5745 (2018).
41. Gao S, Zhou Z, Zhang Y, Deng KK, Feng LS. High-resolution micro-grating accelerometer based on a gram-scale proof mass. *Opt. Express* **27**, 34298–34311 (2019).
42. Li H, Deng KK, Gao S, Feng LS. Design of closed-loop parameters with high dynamic performance for micro-grating accelerometer. *IEEE Access* **7**, 151939–151947 (2019).
43. Zhang Y, Feng LS, Wang X, Wang YJ. Linearity enhancement of scale factor in an optical interrogated micromechanical accelerometer. *Appl Opt* **55**, 6115–6120 (2016).
44. Lu QB, Wang C, Bai J, Wang KW, Lou SQ et al. Minimizing cross-axis sensitivity in grating-based optomechanical accelerometers. *Opt Express* **24**, 9094–9111 (2016).
45. Lu QB, Bai J, Wang KW, He SL. Design, optimization, and realization of a high-performance MOEMS accelerometer from a double-device-layer SOI wafer. *J Microelectromech Syst* **26**, 859–869 (2017).
46. Hall NA, Okandan M, Degertekin FL. Surface and bulk-silicon-micromachined optical displacement sensor fabricated with the SwIFT-Lite™ process. *J Microelectromech Syst* **15**, 770–776 (2006).
47. Berkoff TA, Kersey AD. Experimental demonstration of a fiber Bragg grating accelerometer. *IEEE Photonics Technol Lett* **8**, 1677–1679 (1996).

48. Linze N, Tihon P, Verlinden O, Mégret P, Wuilpart M. Development of a multi-point polarization-based vibration sensor. *Opti Express* **21**, 5606–5624 (2013).
49. Li TL, Shi CY, Ren HL. A novel fiber Bragg grating displacement sensor with a sub-micrometer resolution. *IEEE Photonics Technol Lett* **29**, 1199–1202 (2017).
50. Mita A, Yokoi I. Fiber Bragg grating accelerometer for buildings and civil infrastructures. *Proc SPIE* **4330**, 479–486 (2001).
51. Weng YY, Qiao XG, Guo T, Hu ML, Feng ZY et al. A robust and compact fiber Bragg grating vibration sensor for seismic measurement. *IEEE Sens J* **12**, 800–804 (2012).
52. Munendhar P, Khijwania SK. Two dimensional fiber Bragg grating based vibration sensor for structural health monitoring. *AIP Conference Proceedings* **1536**, 1324–1326 (2013).
53. Peng BJ, Zhao Y, Zhao Y, Yang J. Tilt sensor with FBG technology and matched FBG demodulating method. *IEEE Sens J* **6**, 63–66 (2006).
54. Guan BO, Tam HY, Liu SY. Temperature-independent fiber Bragg grating tilt sensor. *IEEE Photonics Technol Lett* **16**, 224–226 (2004).
55. Bao HL, Dong XY, Gong HP, Chan CC, Shum P. Temperature-insensitive FBG tilt sensor with a large measurement range. In *Proceedings of 2009 Asia Communications and Photonics conference and Exhibition (ACP)* 1–5 (IEEE, 2009). DOI: 10.1117/12.851427
56. He SL, Dong XY, Ni K, Jin YX, Chan C et al. Temperature-insensitive 2D tilt sensor with three fiber Bragg gratings. *Meas Sci Technol* **21**, 025203 (2010).
57. Dong XY, Zhan C, Hu K, Shum P, Chan CC. Temperature-insensitive tilt sensor with strain-chirped fiber Bragg gratings. *IEEE Photonics Technol Lett* **17**, 2394–2396 (2005).
58. Ferdinand P. Optical fiber Bragg grating inclinometry for smart civil engineering and public works. *Proc SPIE* **41855**, 41855O (2000).
59. Aneesh R, Maharana M, Munendhar P, Tam HY, Khijwania SK. Simple temperature insensitive fiber Bragg grating based tilt sensor with enhanced tunability. *Appl Opt* **50**, E172–E176 (2011).
60. Bao HL, Dong XY, Shao LY, Zhao CL, Jin SZ. Temperature-insensitive 2-D tilt sensor by incorporating fiber Bragg gratings with a hybrid pendulum. *Opt Commun* **283**, 5021–5024 (2010).
61. Fernandes CS, Giraldi MTMR, de Sousa MJ, Costa JCWA, Gouveia C et al. Curvature and vibration sensing based on core diameter mismatch structures. *IEEE Trans Instrum Meas* **65**, 2120–2128 (2016).
62. Li K, Chan THT, Yau MH, Nguyen T, Thambiratnam DP et al. Very sensitive fiber Bragg grating accelerometer using transverse forces with an easy over-range protection and low cross axial sensitivity. *Appl Opt* **52**, 6401–6410 (2013).
63. Li TL, Shi CY, Tan YG, Li RY, Zhou ZD et al. A diaphragm type fiber Bragg grating vibration sensor based on transverse property of optical fiber with temperature compensation. *IEEE Sens J* **17**, 1021–1029 (2017).
64. Erdogan T, Sipe JE. Tilted fiber phase gratings. *J Opt Soc Am A* **13**, 296–313 (1996).
65. Lee KS, Erdogan T. Fiber mode coupling in transmissive and reflective tilted fiber gratings. *Appl Opt* **39**, 1394–1404 (2000).
66. Kang SC, Kim SY, Lee SB, Kwon SW, Choi SS et al. Temperature-independent strain sensor system using a tilted fiber Bragg grating demodulator. *IEEE Photonics Technol Lett* **10**, 1461–1463 (1998).
67. Laffont G, Ferdinand P, Technology. Tilted short-period fibre-Bragg-grating-induced coupling to cladding modes for accurate refractometry. *Meas Sci Technol* **12**, 765–770 (2001).
68. Shevchenko YY, Albert J. Plasmon resonances in gold-coated tilted fiber Bragg gratings. *Opt Lett* **32**, 211–213 (2007).
69. Chehura E, James SW, Tatam RP. Temperature and strain discrimination using a single tilted fibre Bragg grating. *Opt Commun* **275**, 344–347 (2007).
70. Zhou B, Zhang AP, He SL, Gu BB. Cladding-mode-recoupling-based tilted fiber Bragg grating sensor with a core-diameter-mismatched fiber section. *IEEE Photonics J* **2**, 152–157 (2010).
71. Helan R, Urban Jr F, Mikel B, Sr FU. Preparation and measurement of TFBG based vibration sensor. *Proc SPIE* **92864**, 92864D (2014).
72. Huang YH, Guo TA, Lu C, Tam HY. Vcsel-based tilted fiber grating vibration sensing system. *IEEE Photonics Technol Lett* **22**, 1235–1237 (2010).
73. Shao LY, Xiong LY, Chen CK, Laronche A, Albert J. Directional bend sensor based on re-grown tilted fiber Bragg grating. *J Lightwave Technol* **28**, 2681–2687 (2010).
74. Shao LY, Albert J. Compact fiber-optic vector inclinometer. *Opt Lett* **35**, 1034–1036 (2010).
75. Basumallick N, Chatterjee I, Biswas P, Dasgupta K, Bandyopadhyay S. Fiber Bragg grating accelerometer with enhanced sensitivity. *Sens Actuat A-Phys* **173**, 108–115 (2012).
76. Basumallick N, Biswas P, Dasgupta K, Bandyopadhyay S. Design optimization of fiber Bragg grating accelerometer for maximum sensitivity. *Sens Actuat A-Phys* **194**, 31–39 (2013).
77. Khan MM, Panwar N, Dhawan R. Modified cantilever beam shaped FBG based accelerometer with self temperature compensation. *Sens Actuat A-Phys* **205**, 79–85 (2014).
78. Liu QP, Qiao XG, Jia ZA, Fu HW, Gao H et al. Large frequency range and high sensitivity fiber Bragg grating accelerometer based on double diaphragms. *IEEE Sens J* **14**, 1499–1504 (2014).
79. Liu QP, Qiao XG, Zhao JL, Jia ZA, Gao H et al. Novel fiber Bragg grating accelerometer based on diaphragm. *IEEE Sens J* **12**, 3000–3004 (2012).
80. Zhu YN, Shum P, Lu C, Lacquet BM, Swart PL et al. Temperature-insensitive fiber Bragg grating accelerometer. *IEEE Photonics Technol Lett* **15**, 1437–1439 (2003).
81. Zhou WJ, Dong XY, Shen CY, Zhao CL, Chan CC et al. Temperature-independent vibration sensor with a fiber bragg grating. *Microw Opt Technol Lett* **52**, 2282–2285 (2010).
82. Todd MD, Johnson GA, Althouse BA, Vohra ST. Flexural beam-based fiber Bragg grating accelerometers. *IEEE Photonics Technol Lett* **10**, 1605–1607 (1998).
83. Gutiérrez N, Galvín P, Lasagni F. Low weight additive manufacturing FBG accelerometer: design, characterization and testing. *Measurement* **117**, 295–303 (2018).
84. Li K, Liu GY, Li YQ, Yang J, Ma WL. Ultra-small fiber bragg grating accelerometer. *Appl Sci* **9**, 2707 (2019).
85. Wei L, Jiang DZ, Yu LL, Li HC, Liu Z. A novel miniaturized fiber bragg grating vibration sensor. *IEEE Sens J* **19**, 11932–11940 (2019).

86. Gerges AS, Newson TP, Jackson DA. Practical fiber-optic-based submicro-*g* accelerometer free from source and environmental perturbations. *Appl Sci* **14**, 1155–1157 (1989).
87. Stephens M. A sensitive interferometric accelerometer. *Rev Sci Instrum* **64**, 2612–2614 (1993).
88. Wang DH, Jia PG. Fiber optic extrinsic Fabry-Perot accelerometer using laser emission frequency modulated phase generated carrier demodulation scheme. *Opt Eng* **52**, 055004 (2013).
89. Gerges AS, Newson TP, Jones JDC, Jackson DA. High-sensitivity fiber-optic accelerometer. *Opt Lett* **14**, 251–253 (1989).
90. Lin QA, Chen LH, Li S, Wu X. A high-resolution fiber optic accelerometer based on intracavity phase-generated carrier (PGC) modulation. *Meas Sci Technology* **22**, 015303 (2011).
91. Yu B, Wang AB, Pickrell GR. Analysis of fiber Fabry-Pérot interferometric sensors using low-coherence light sources. *J Lightwave Technol* **24**, 1758–1767 (2006).
92. Guo JJ, Yang CX. Non-contact fiber vibration sensor based on intracavity modulation of an extrinsic Fabry-Perot interferometer. *IEEE Sens J* **15**, 7229–7233 (2015).
93. Liu B, Lin J, Liu H, Ma Y, Yan L et al. Diaphragm based long cavity Fabry-Perot fiber acoustic sensor using phase generated carrier. *Opt Commun* **382**, 514–518 (2017).
94. Jia PG, Wang DH. Temperature-compensated fiber optic Fabry-Perot accelerometer based on the feedback control of the Fabry-Perot cavity length. *Chin Opt Lett* **11**, 8–12 (2013).
95. Wang XD, Li BQ, Xiao ZX, Lee SH, Roman H et al. An ultrasensitive optical MEMS sensor for partial discharge detection. *J Micromech Microeng* **15**, 521–527 (2005).
96. Davies E, George DS, Gower MC, Holmes AS. MEMS Fabry-Pérot optical accelerometer employing mechanical amplification via a V-beam structure. *Sens Actuat A-Phys* **215**, 22–29 (2014).
97. Zhao ZH, Yu ZH, Chen K, Yu QX. A fiber-optic fabry-perot accelerometer based on high-speed white light interferometry demodulation. *J Lightwave Technol* **36**, 1562–1567 (2018).
98. Kippenberg TJ, Vahala KJ. Cavity optomechanics: back-action at the mesoscale. *Science* **321**, 1172–1176 (2008).
99. Aspelmeyer M, Kippenberg TJ, Marquardt F. Cavity optomechanics. *Rev Mod Phys* **86**, 1391–1452 (2014).
100. Bowen WP, Milburn GJ. *Quantum Optomechanics*. (CRC Press, Boca Raton, 2015).
101. Meystre P. A short walk through quantum optomechanics. *Ann Phys* **525**, 215–233 (2013).
102. Maimaiti W, Li Z, Chesi S, Wang Y. Entanglement concentration with strong projective measurement in an optomechanical system. *SCIENCE CHINA Physics, Mechanics & Astronomy* **58**, 1–6 (2015). DOI: 10.1007/s11433-015-5657-8
103. Cervantes FG, Kumanchik L, Pratt J, Taylor JM. High sensitivity optomechanical reference accelerometer over 10 kHz. *Appl Phys Lett* **104**, 221111 (2014).
104. Bao YL, Cervantes FG, Balijepalli A, Lawall JR, Taylor JM et al. An optomechanical accelerometer with a high-finesse hemispherical optical cavity. In *Proceedings of 2016 IEEE International Symposium on Inertial Sensors and Systems* 105–108 (IEEE, 2016); http://doi.org/10.1109/ISISS.2016.7435556.
105. Gerberding O, Cervantes FG, Melcher J, Pratt JR, Taylor JM. Optomechanical reference accelerometer. *Metrologia* **52**, 654–665 (2015).
106. Li J, Sun JN, Miliar MM, Dong FZ, Maier RRJ et al. Two-dimensional optical fibre cantilever accelerometer. *Proc SPIE* **96341**, 96341E (2015).
107. Liu B, Zhong Z, Lin J, Wang X, Liu L et al. Extrinsic Fabry-Perot cantilever accelerometer based on micromachined 45° angled fiber. *J Lightwave Technol* **36**, 2196–2203 (2018).
108. Han J, Zhang WT, Wang ZG, Sun BC, Xu BH et al. Fiber optical accelerometer based on 45 degrees Fabry-Perot cavity. *Proc SPIE* **9274**, 927418 (2014).
109. Zeng N, Shi CZ, Zhang M, Wang LW, Liao YB et al. A 3-component fiber-optic accelerometer for well logging. *Opt Commun* **234**, 153–162 (2004).
110. Morikawa SRK, Ribeiro AS, Regazzi RD, Valente LCG, Braga AMB. Triaxial Bragg grating accelerometer. In *Proceedings of the 15th Optical Fiber Sensors Conference Technical Digest. OFS 2002(Cat. No.02EX533)* 95 –98 (IEEE, 2002); http://doi.org/10.1109/OFS.2002.1000510.
111. Amarasinghe R, Dao DV, Toriyama T, Sugiyama S. Design and fabrication of a miniaturized six-degree-of-freedom piezoresistive accelerometer. *J Micromech Microeng* **15**, 1745–1753 (2005).
112. Amarasinghe R, Dao DV, Toriyama T, Sugiyama S. Development of miniaturized 6-axis accelerometer utilizing piezoresistive sensing elements. *Sens Actuat A-Phys* **134**, 310–320 (2007).
113. Sirkis JS, Brennan DD, Putman MA, Berkoff TA, Kersey AD et al. In-line fiber etalon for strain measurement. *Opt Lett* **18**, 1973–1975 (1993).
114. Liu WL, Li WZ, Yao JP. Real-time interrogation of a linearly chirped fiber Bragg grating sensor for simultaneous measurement of strain and temperature. *IEEE Photonics Technol Lett* **23**, 1340–1342 (2011).
115. Echevarria J, Quintela A, Jauregui C, Lopez-Higuera JM. Uniform fiber Bragg grating first-and second-order diffraction wavelength experimental characterization for strain-temperature discrimination. *IEEE Photonics Technol Lett* **13**, 696–698 (2001).
116. Shao LY, Dong XY, Zhang AP, Tam HY, He SL. High-resolution strain and temperature sensor based on distributed Bragg reflector fiber laser. *IEEE Photonics Technol Lett* **19**, 1598–1600 (2007).
117. Rong QZ, Sun H, Qiao XG, Zhang J, Hu ML et al. A miniature fiber-optic temperature sensor based on a Fabry–Perot interferometer. *J Opt* **14**, 045002 (2012).
118. Fender A, MacPherson WN, Maier RRJ, Barton JS, George DS et al. Two-axis temperature-insensitive accelerometer based on multicore fiber Bragg gratings. *IEEE Sens J* **8**, 1292–1298 (2008).
119. Zhao CL, Yang X, Demokan M, Jin W. Simultaneous temperature and refractive index measurements using a 3°slanted multimode fiber Bragg grating. *J. Lightwave Technol* **24**, 879–883 (2006).
120. Zhang Q, Zhu T, Hou YS, Chiang KS. All-fiber vibration sensor based on a Fabry–Perot interferometer and a microstructure beam. *J Opt Soc Am B* **30**, 1211–1215 (2013).
121. Gagliardi G, Salza M, Ferraro P, De Natale P, Di Maio A et al. Design and test of a laser-based optical-fiber Bragg-grating accelerometer for seismic applications. *Meas Sci Technol* **19**, 085306 (2008).

122. Tsuda H. Fiber Bragg grating vibration-sensing system, insensitive to Bragg wavelength and employing fiber ring laser. *Opt Lett* **35**, 2349–2351 (2010).
123. Ma WY, Jiang Y, Zhang H, Zhang LC, Hu J et al. Miniature on-fiber extrinsic Fabry-Perot interferometric vibration sensors based on micro-cantilever beam. *Nanotechnol Rev* **8**, 293–298 (2019).
124. Lee YG, Kim DH, Kim CG. Performance of a single reflective grating-based fiber optic accelerometer. *Meas Sci Technol* **23**, 045101 (2012).
125. Ferreira MS, Coelho L, Schuster K, Kobelke J, Santos JL et al. Fabry –Perot cavity based on a diaphragm-free hollow-core silica tube. *Opt Lett* **36**, 4029–4031 (2011).
126. Xiao GZ, Adnet A, Zhang ZY, Sun FG, Grover CP. Monitoring changes in the refractive index of gases by means of a fiber optic Fabry-Perot interferometer sensor. *Sens Actuat A-Phys* **118**, 177–182 (2005).
127. Amarasinghe R, Dao DV, Toriyama T, Sugiyama S. Simulation, fabrication and characterization of a three-axis piezoresistive accelerometer. *Smart Mater Struct* **15**, 1691–1699 (2006).
128. Rao YJ, Henderson PJ, Jackson DA, Zhang L, Bennion I. Simultaneous strain, temperature and vibration measurement using a multiplexed in-fibre-Bragg-grating/fibre-Fabry-Perot sensor system. *Electron Lett* **33**, 2063–2064 (1997).
129. Yu YL, Tam H, Chung W, Demokan MS. Fiber Bragg grating sensor for simultaneous measurement of displacement and temperature. *Opt Lett* **25**, 1141–1143 (2000).
130. Jia PG, Wang DH, Yuan G, Jiang XY. An active temperature compensated fiber-optic Fabry-Perot accelerometer system for simultaneous measurement of vibration and temperature. *IEEE Sens J* **13**, 2334–2340 (2013).
131. Corres JM, Bravo J, Arregui FJ, Matias IR. Vibration monitoring in electrical engines using an in-line fiber etalon. *Sens Actuat A-Phys* **132**, 506–515 (2006).
132. Ke T, Zhu T, Rao YJ, Deng M. Accelerometer based on all-fiber Fabry-Pérot interferometer formed by hollow-core photonic crystal fiber. *Microw Opt Technol Lett* **52**, 2531–2535 (2010).
133. Zang ZG, Yang WX. Theoretical and experimental investigation of all-optical switching based on cascaded LPFGs separated by an erbium-doped fiber. *J Appl Phys* **109**, 103106 (2011).
134. Zang ZJ. Numerical analysis of optical bistability based on fiber Bragg grating cavity containing a high nonlinearity doped-fiber. *Opt Commun* **285**, 521–526 (2012).
135. Zang ZG, Zhang YJ. Low-switching power (< 45 mW) optical bistability based on optical nonlinearity of ytterbium-doped fiber with a fiber Bragg grating pair. *J Mod Opt* **59**, 161–165 (2012).
136. Xu JC, Wang XW, Cooper KL, Wang AB. Miniature all-silica fiber optic pressure and acoustic sensors. *Opt Lett* **30**, 3269–3271 (2005).
137. Wang DH, Wang SJ, Jia PG. In-line silica capillary tube all-silica fiber-optic Fabry–Perot interferometric sensor for detecting high intensity focused ultrasound fields. *Opt Lett* **37**, 2046–2048 (2012).
138. Jaksic Z, Radulovic K, Tanaskovic D. MEMS accelerometer with all-optical readout based on twin-defect photonic crystal waveguide. In *Proceedings of the 24th International Conference on Microelectronics* 231 –234 (IEEE, 2004); http://doi.org/10.1109/ICMEL.2004.1314602.
139. Huang K, Yu M, Cheng L, Liu J, Cao LQ. A proposal for an optical MEMS accelerometer with high sensitivity based on wavelength modulation system. *J Lightwave Technol* **37**, 5474–5478 (2019).
140. Huang K, Cao LQ, Zhai PC, Liu PY, Cheng L et al. High sensitivity sensing system theoretical research base on waveguide-nano DBRs one dimensional photonic crystal microstructure. *Opt Commun* **470**, 125392 (2020).
141. Sheikhaleh A, Abedi K, Jafari K. An Optical MEMS Accelerometer based on a two-dimensional photonic crystal add-drop filter. *J Lightwave Technol* **35**, 3029–3034 (2017).
142. Sheikhaleh A, Abedi K, Jafari K. A proposal for an optical mems accelerometer relied on wavelength modulation with one dimensional photonic crystal. *J Lightwave Technol* **34**, 5244–5249 (2016).
143. Olyaee S, Azizi M. Micro-displacement sensor based on high sensitivity photonic crystal. *Photonic Sens* **4**, 220–224 (2014).
144. Ritchie RH, Marusak AL. Surface plasmon dispersion relation for an electron gas. *Surf Sci* **4**, 234–240 (1966).
145. Ebbesen TW, Lezec HJ, Ghaemi HF, Thio T, Wolff PA. Extraordinary optical transmission through sub-wavelength hole arrays. *Nature* **391**, 667–669 (1998).
146. Nemati A, Wang Q, Hong MH, Teng JH. Tunable and reconfigurable metasurfaces and metadevices. *Opto-Electron Adv* **1**, 180009 (2018).
147. Carr DW, Sullivan JP, Friedmann TA. Laterally deformable nanomechanical zeroth-order gratings: anomalous diffraction studied by rigorous coupled-wave analysis. *Opt Lett* **28**, 1636–1638 (2003).
148. Keeler BEN, Bogart GR, Carr DW. Laterally deformable optical NEMS grating transducers for inertial sensing applications. *Proc SPIE* **5592**, 306–312 (2005).
149. Krishnamoorthy U, Olsson III RH, Bogart GR, Baker MS, Carr DW et al. In-plane MEMS-based nano-g accelerometer with sub-wavelength optical resonant sensor. *Sens Actuat A-Phys* **145-146**, 283–290 (2008).
150. Krause AG, Winger M, Blasius TD, Lin Q, Painter O. A high-resolution microchip optomechanical accelerometer. *Nat Photonics* **6**, 768–772 (2012).
151. Eichenfield M, Camacho R, Chan J, Vahala KJ, Painter O. A picogram- and nanometre-scale photonic-crystal optomechanical cavity. *Nature* **459**, 550–555 (2009).
152. Lin Q, Rosenberg J, Jiang XS, Vahala KJ, Painter O. Mechanical oscillation and cooling actuated by the optical gradient force. *Phys Rev Lett* **103**, 103601 (2009).
153. Safavi-Naeini AH, Gröblacher S, Hill JT, Chan J, Aspelmeyer M et al. Squeezed light from a silicon micromechanical resonator. *Nature* **500**, 185–189 (2013).
154. Kim PH, Hauer BD, Doolin C, Souris F, Davis JP. Approaching the standard quantum limit of mechanical torque sensing. *Nat Commun* **7**, 13165 (2016).
155. Zobenica Z, van der Heijden RW, Petruzzella M, Pagliano F, Leijssen R et al. Integrated nano-opto-electro-mechanical sensor for spectrometry and nanometrology. *Nat Commun* **8**, 2216 (2017).
156. Huang YJ, Flor Flores JG, Li Y, Wang WT, Wang D et al. A

chip-scale oscillation-mode optomechanical inertial sensor near the thermodynamical limits. *Laser Photonics Rev* **14**, 1800329 (2020).
157. Rogers AAA, Kedia S, Samson S, Bhansali S. Verification of evanescent coupling from subwavelength grating pairs. *Appl Phys B* **105**, 833–837 (2011).
158. Yao BY, Feng LS, Wang X, Liu MH, Zhou Z et al. Design of out-of-plane MOEMS accelerometer with subwavelength gratings. *IEEE Photonics Technol Lett* **26**, 1027–1030 (2014).
159. Lu QB, Bai J, Wang KW, Chen PW, Fang WD et al. Single Chip-based nano-optomechanical accelerometer based on subwavelength grating pair and rotated serpentine springs. *Sensors* **18**, 2036 (2018).
160. Snadden MJ, McGuirk JM, Bouyer P, Haritos KG, Kasevich MA. Measurement of the Earth's gravity gradient with an atom interferometer-based gravity gradiometer. *Phys Rev Lett* **81**, 971–974 (1998).
161. Peters A, Chung KY, Chu S. High-precision gravity measurements using atom interferometry. *Metrologia* **38**, 25–61 (2001).
162. McGuirk JM, Foster GT, Fixler JB, Snadden MJ, Kasevich MA. Sensitive absolute-gravity gradiometry using atom interferometry. *Phys Rev A* **65**, 033608 (2002).
163. Kovachy T, Asenbaum P, Overstreet C, Donnelly CA, Dickerson SM et al. Quantum superposition at the half-metre scale. *Nature* **528**, 530–533 (2015).
164. Armata F, Latmiral L, Plato ADK, Kim MS. Quantum limits to gravity estimation with optomechanics. *Phys Rev A* **96**, 043824 (2017).
165. Qvarfort S, Serafini A, Barker PF, Bose S. Gravimetry through non-linear optomechanics. *Nat Commun* **9**, 3690 (2018).
166. Arvanitaki A, Geraci AA. Detecting high-frequency gravitational waves with optically levitated sensors. *Phys Rev Lett* **110**, 071105 (2013).
167. Gietka K, Mivehvar F, Ritsch H. Supersolid-based gravimeter in a ring cavity. *Phys Rev Lett* **122**, 190801 (2019).
168. Purdy TP, Peterson RW, Regal CA. Observation of radiation pressure shot noise on a macroscopic object. *Science* **339**, 801–804 (2013).
169. Abend S, Gebbe M, Gersemann M, Ahlers H, Müntinga H et al. Atom-chip fountain gravimeter. *Phys Rev Lett* **117**, 203003 (2016).
170. Cheiney P, Fouché L, Templier S, Napolitano F, Battelier B et al. Navigation-compatible hybrid quantum accelerometer using a kalman filter. *Phys Rev Appl* **10**, 034030 (2018).
171. Metcalfe M. Applications of cavity optomechanics. *Appl Phys Rev* **1**, 031105 (2014).

Acknowledgements

We are grateful for financial supports from National Natural Science Foundation of China (No. 62004166), Fundamental Research Funds for the Central Universities (No. 31020190QD027), Natural Science Basic Research Program of Shaanxi (Program No. 2020JQ-199), China National Postdoctoral Program for Innovative Talents (No. BX20200279) and Key Research and Development Program of Shaanxi Province (2020GXLH-Z-027, 2020ZDLGY04-08).

Author contributions

All authors commented on the manuscript. Q. B. Lu and Y. N. Wang drafted manuscript with equal contribution. Q. B. Lu and W. Huang supervised the work and finalized manuscript with inputs of all authors.

Competing interests

The authors declare no competing financial interests.